

Supporting Information for "Potential and Challenges of Investigating Intrinsic Uncertainty of Hydrological Models with Stochastic, Time-Dependent Parameters"

Peter Reichert, Lorenz Ammann, Fabrizio Fenicia

Eawag: Swiss Federal Institute of Aquatic Science and Technology, 8600 Dübendorf, Switzerland

Contents of this file

1. Text S1 to S8
2. Figures S1 to S59

Introduction

This file contains a complete overview of inference and model output results for all five models M1a, M1b, M2a, M2b and M2c for constant (Sections S1 - S3) and stochastic, time-dependent parameters (Sections S4 - S7) and a complete set of scatter plots of the factors, f_{k_i} , as a function of the reservoir levels, S_i (Section S8).

Model with constant parameters:

- S1. Markov chains and 1d marginal densities (Figs. S1 - S5).
- S2. Samples of 2d marginals (Figs. S6 - S10).
- S3. Time series of discharge and states for different time ranges (Figs. S11 - S25).

Model with stochastic, time-dependent parameters:

- S4. Markov chains and 1d marginal densities (Figs. S26 - S30).
- S5. Samples of 2d marginals (Figs. S31 - S35).
- S6. Markov chains and 1d marginals of stochastic parameters at selected time points (Figs. S36 - S43).
- S7. Time series of discharge and states for different time ranges (Figs. S44 - S58).
- S8. Scatter plots of the factors, f_{k_i} , as a function of the reservoir levels, S_i (Fig. S59).

Copyright 2021 by the American Geophysical Union.
0043-1397 /21/\$9.00

Text S1. Markov chains and one-dimensional marginal posterior distributions of parameters of the models without time-dependent parameters

The Figures S1 to S5 show four Markov chains of the model parameters and the corresponding one-dimensional marginal posterior distributions for each of the models M1a, M1b, M2a, M2b and M2c with constant parameters. Each figure shows the 1d projections of the four chains (left) and the corresponding marginal densities (right). The Markov chains were started from previous burn-in runs and thus show nearly no burn-in. The red line indicates the end of the adaptation phase of the Metropolis algorithm, the blue, dashed line marks the iteration at which the evaluation of the chain starts (to be sure not to have remaining burn-in for the the evaluation).

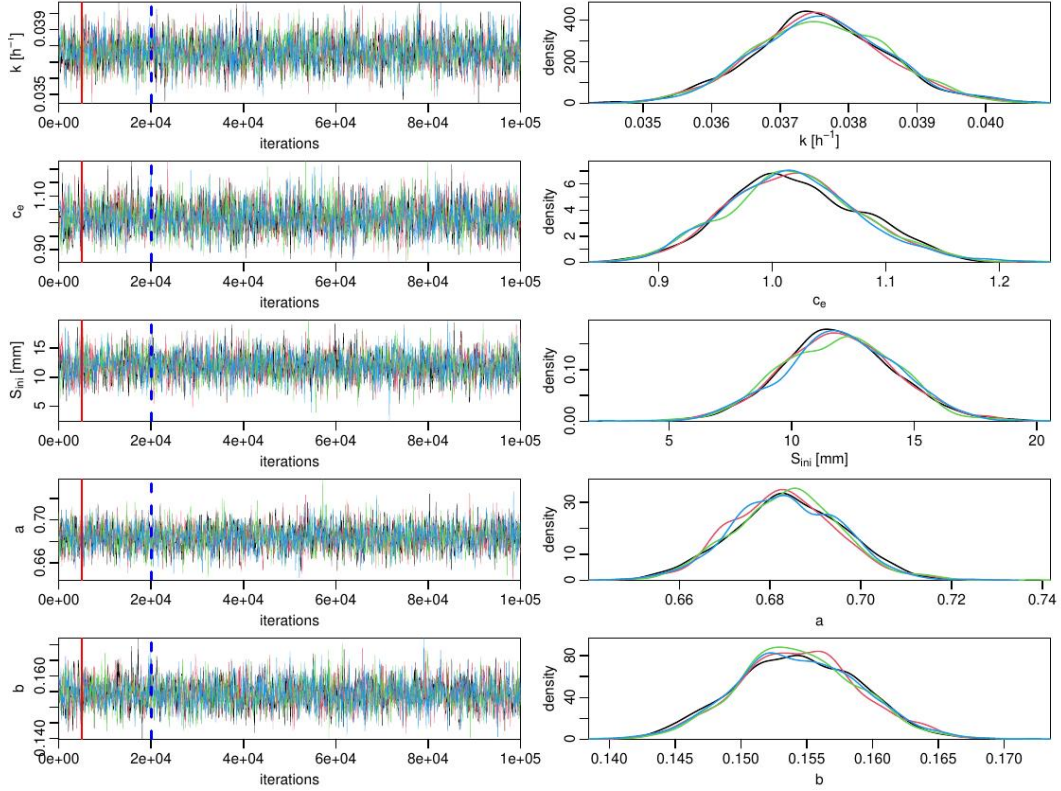


Figure S1. Markov chains and one-dimensional posterior marginals of the parameters of model M1a without time-dependent parameters.

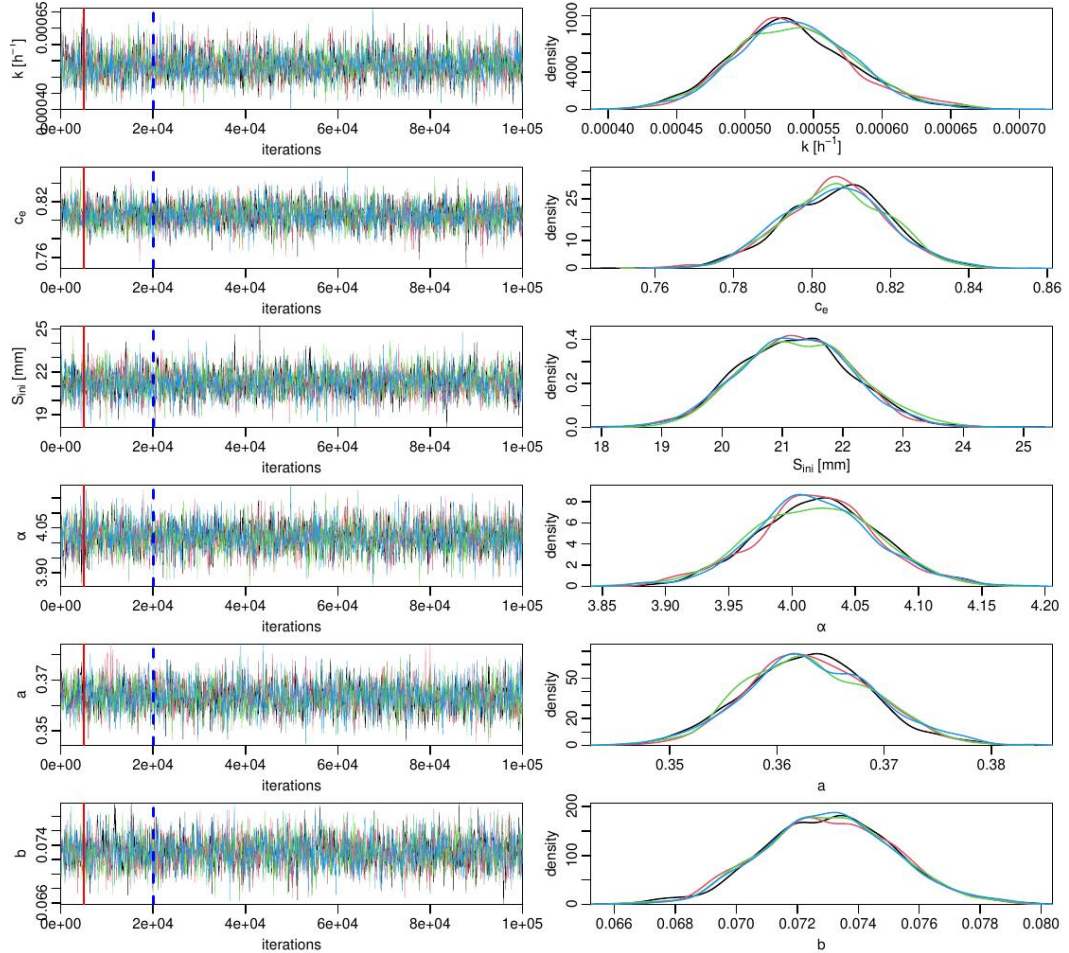


Figure S2. Markov chains and one-dimensional posterior marginals of the parameters of model M1b without time-dependent parameters.

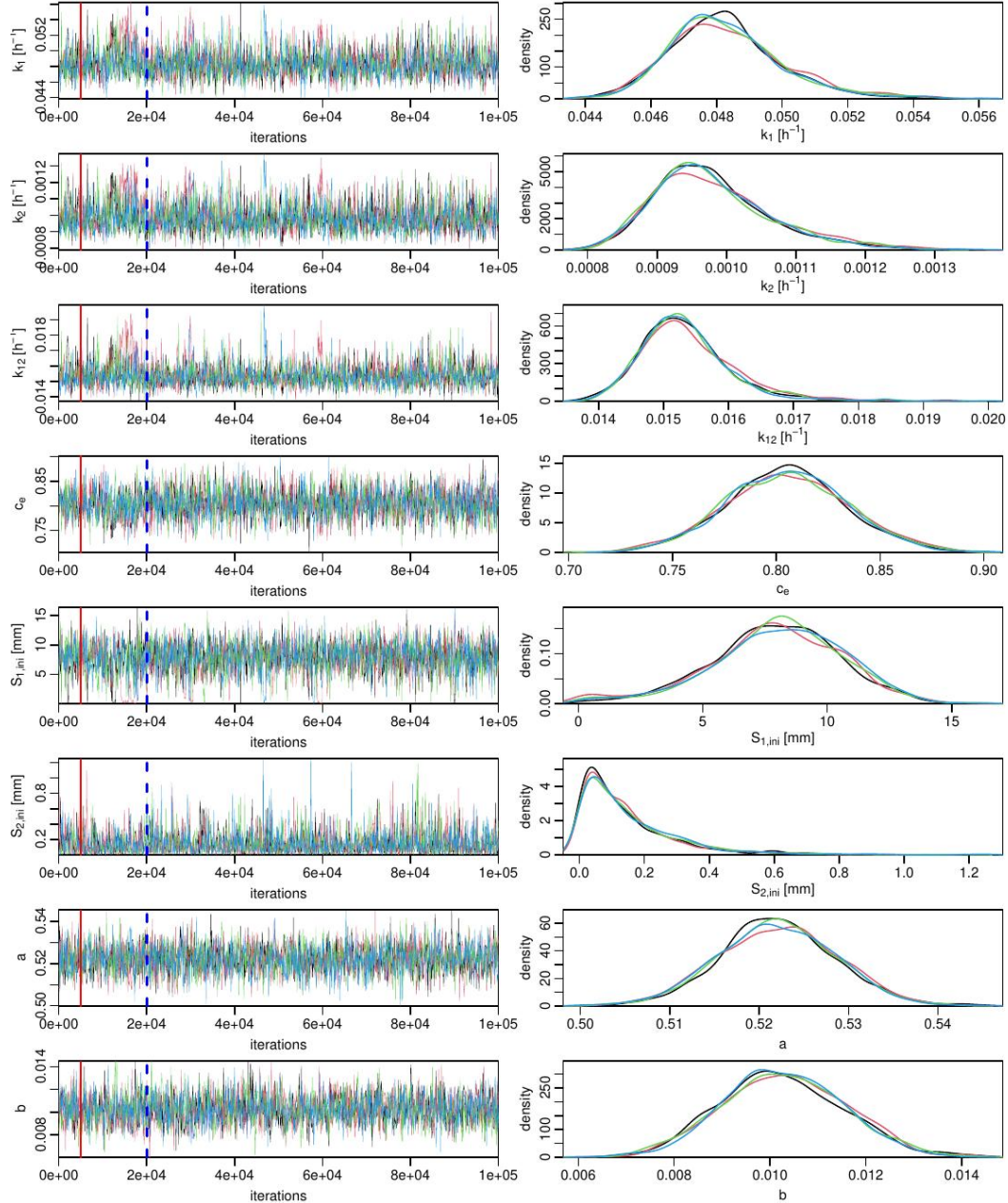


Figure S3. Markov chains and one-dimensional posterior marginals of the parameters of model M2a without time-dependent parameters.

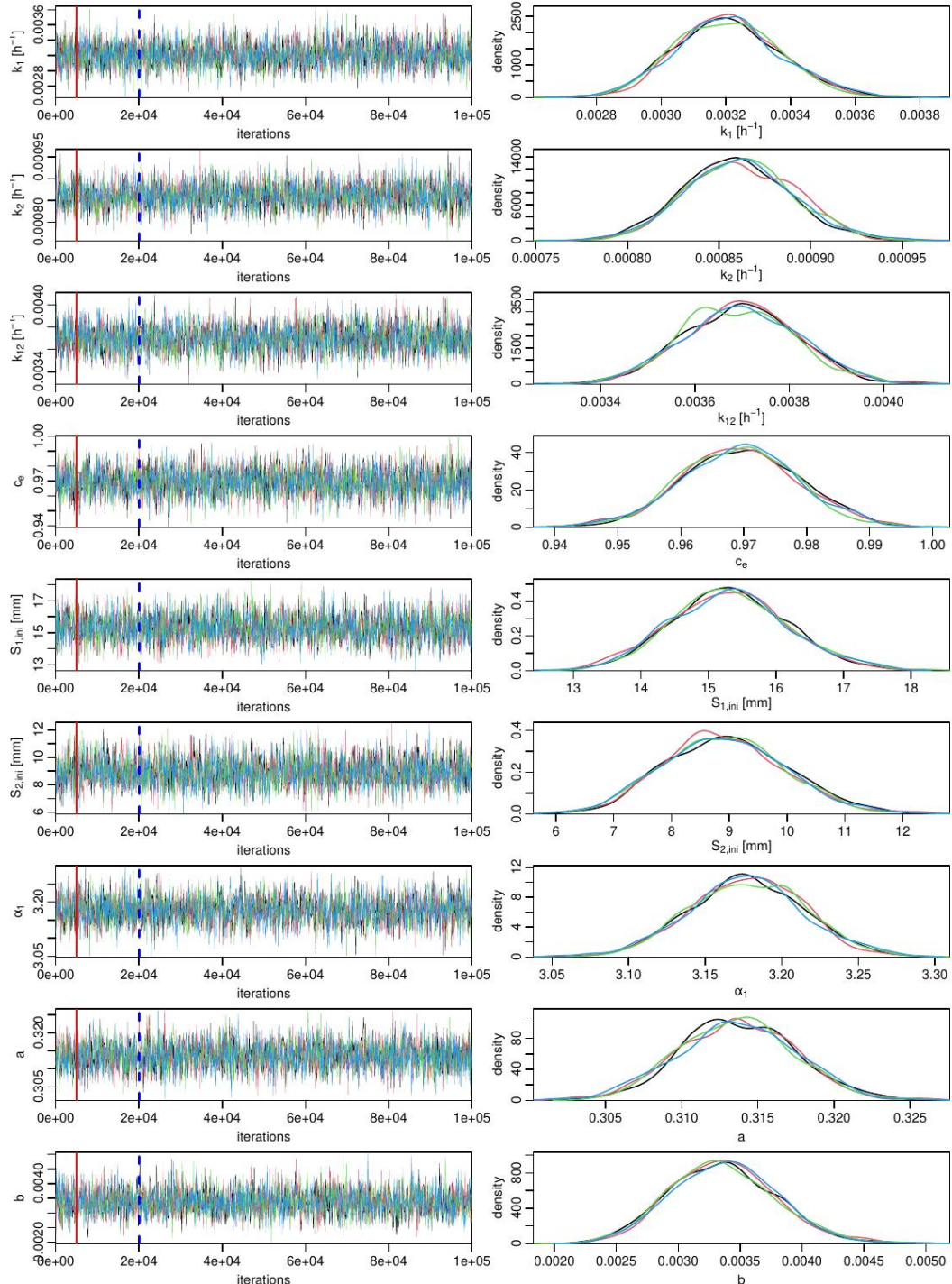


Figure S4. Markov chains and one-dimensional posterior marginals of the parameters of model M2b without time-dependent parameters.

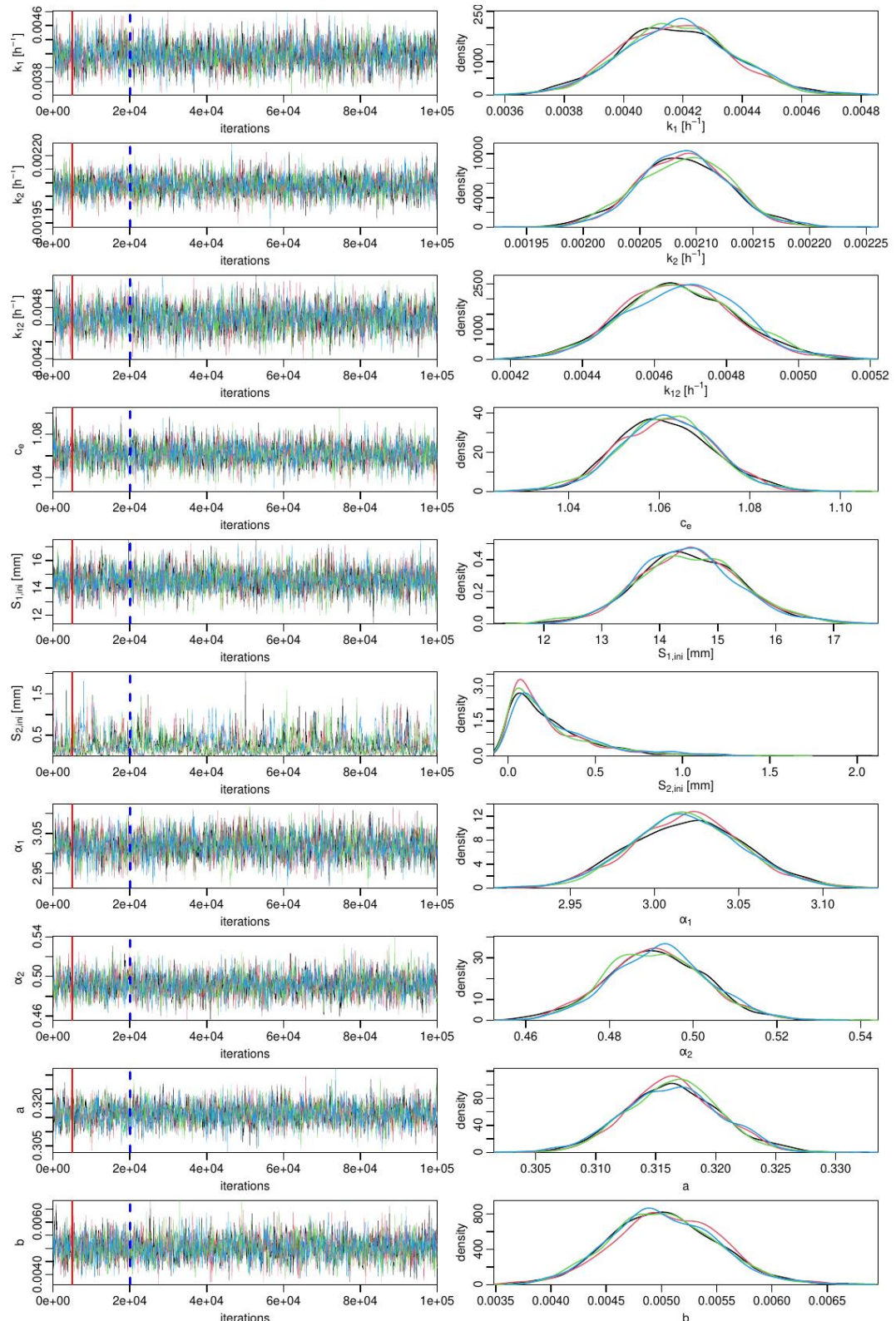


Figure S5. Markov chains and one-dimensional posterior marginals of the parameters of model M2c without time-dependent parameters.

Text S2. Two-dimensional marginal posterior distributions of parameters of the models without time-dependent parameters

The Figures S6 to S10 show two-dimensional marginal posterior samples of four Markov chains of the model parameters for each of the models M1a, M1b, M2a, M2b and M2c with constant parameters.

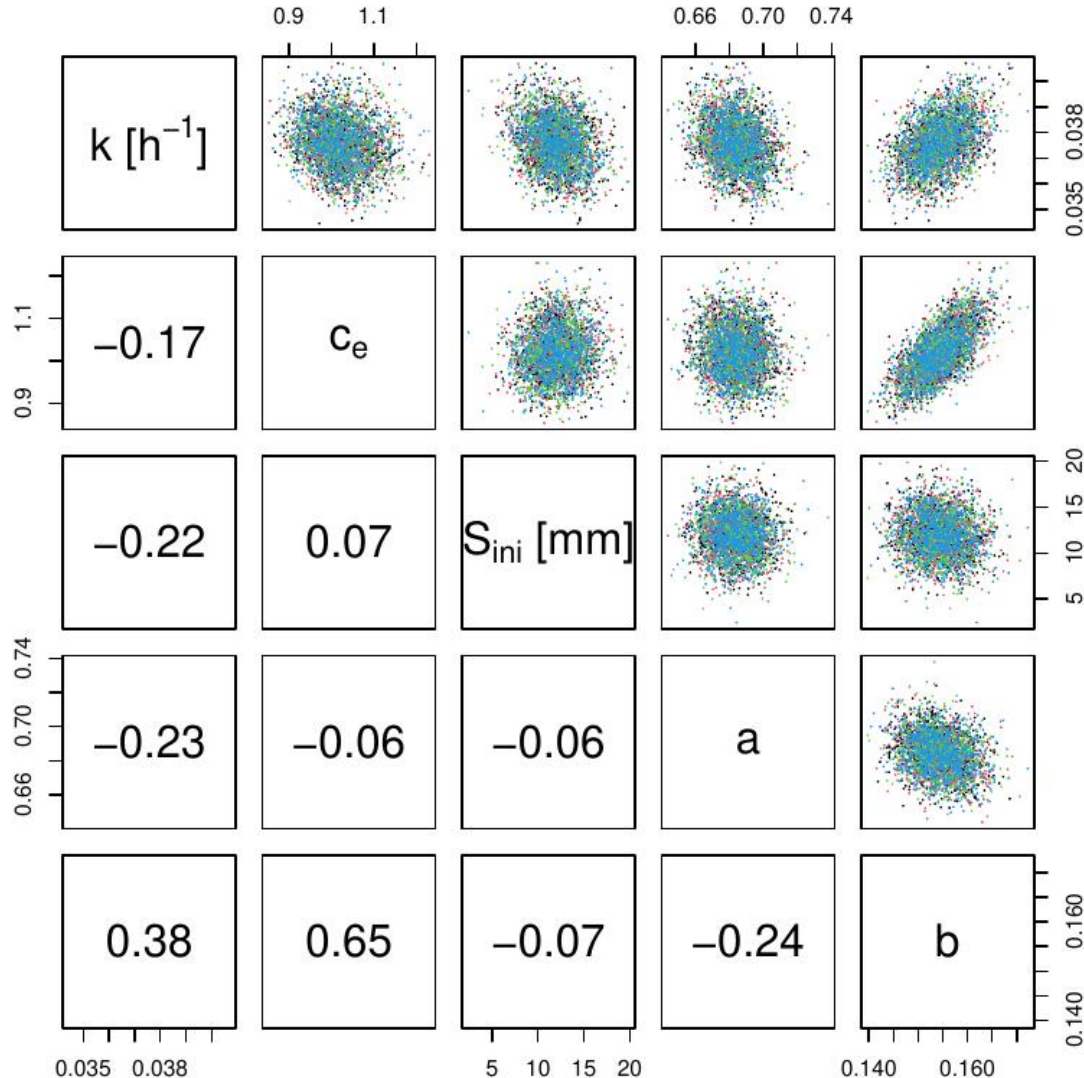


Figure S6. Samples of the two-dimensional posterior marginals of the parameters of model M1a without time-dependent parameters.

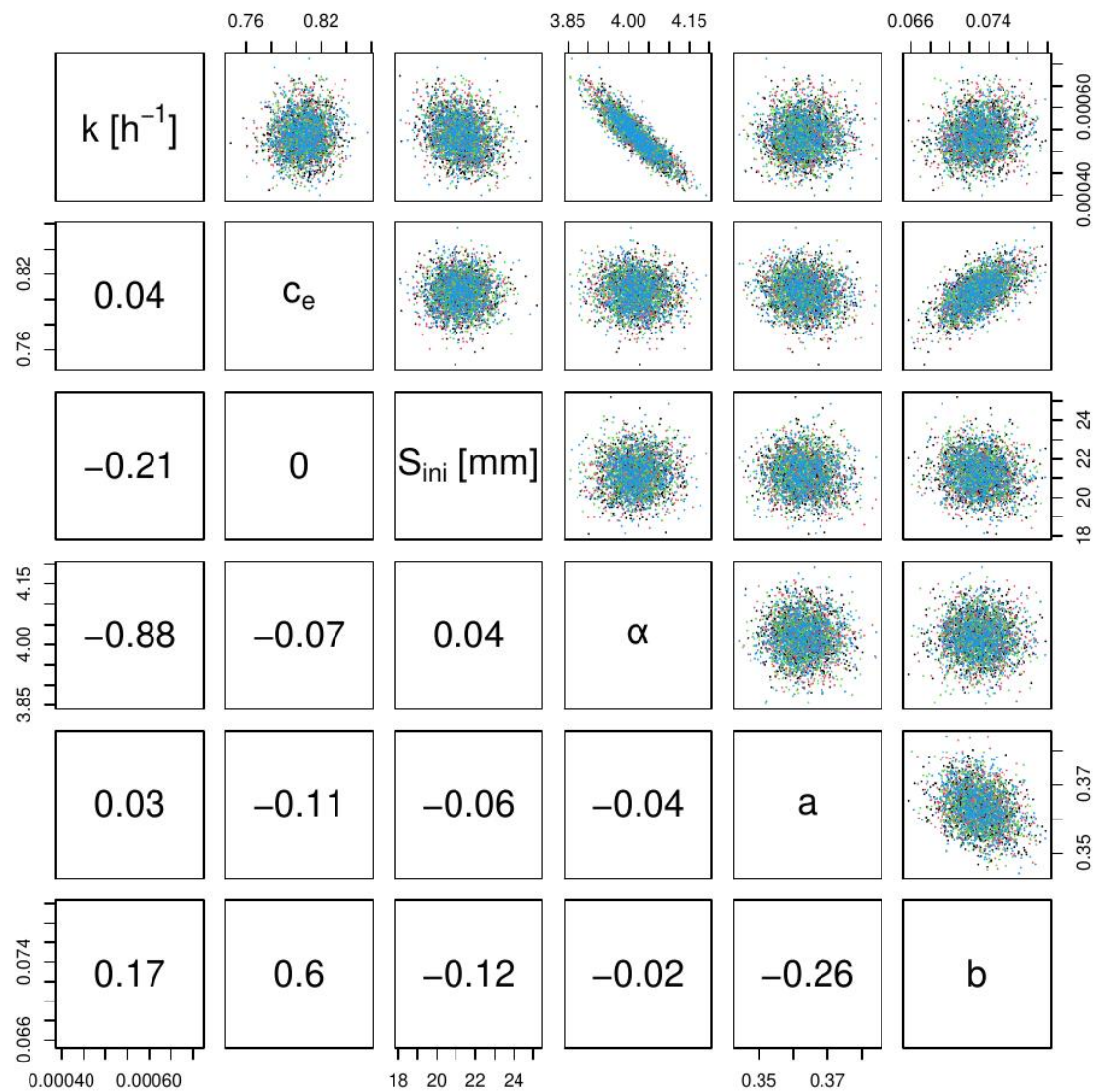


Figure S7. Samples of the two-dimensional posterior marginals of the parameters of model M1b without time-dependent parameters.

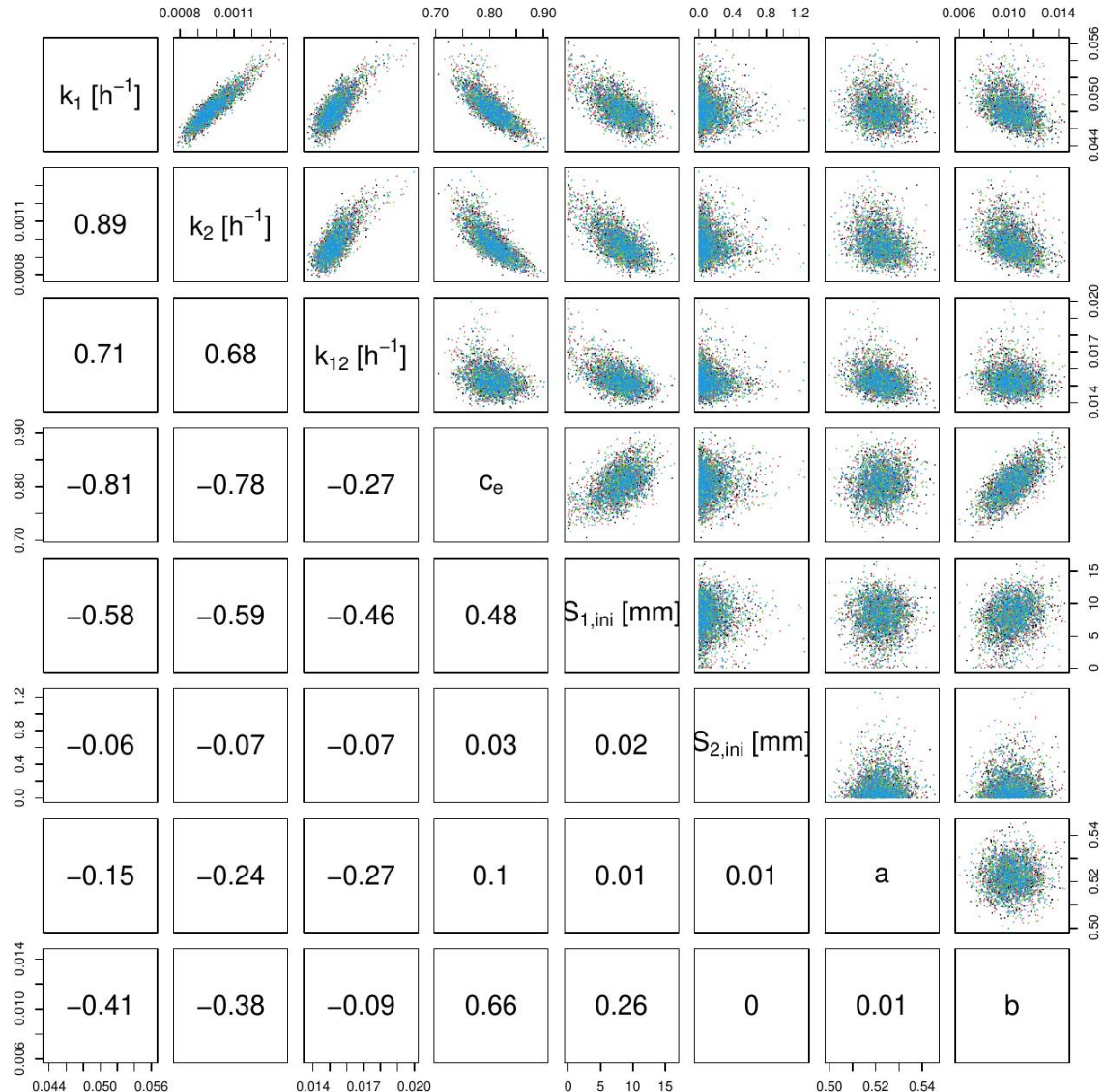


Figure S8. Samples of the two-dimensional posterior marginal distributions of the parameters of model M2a without time-dependent parameters.

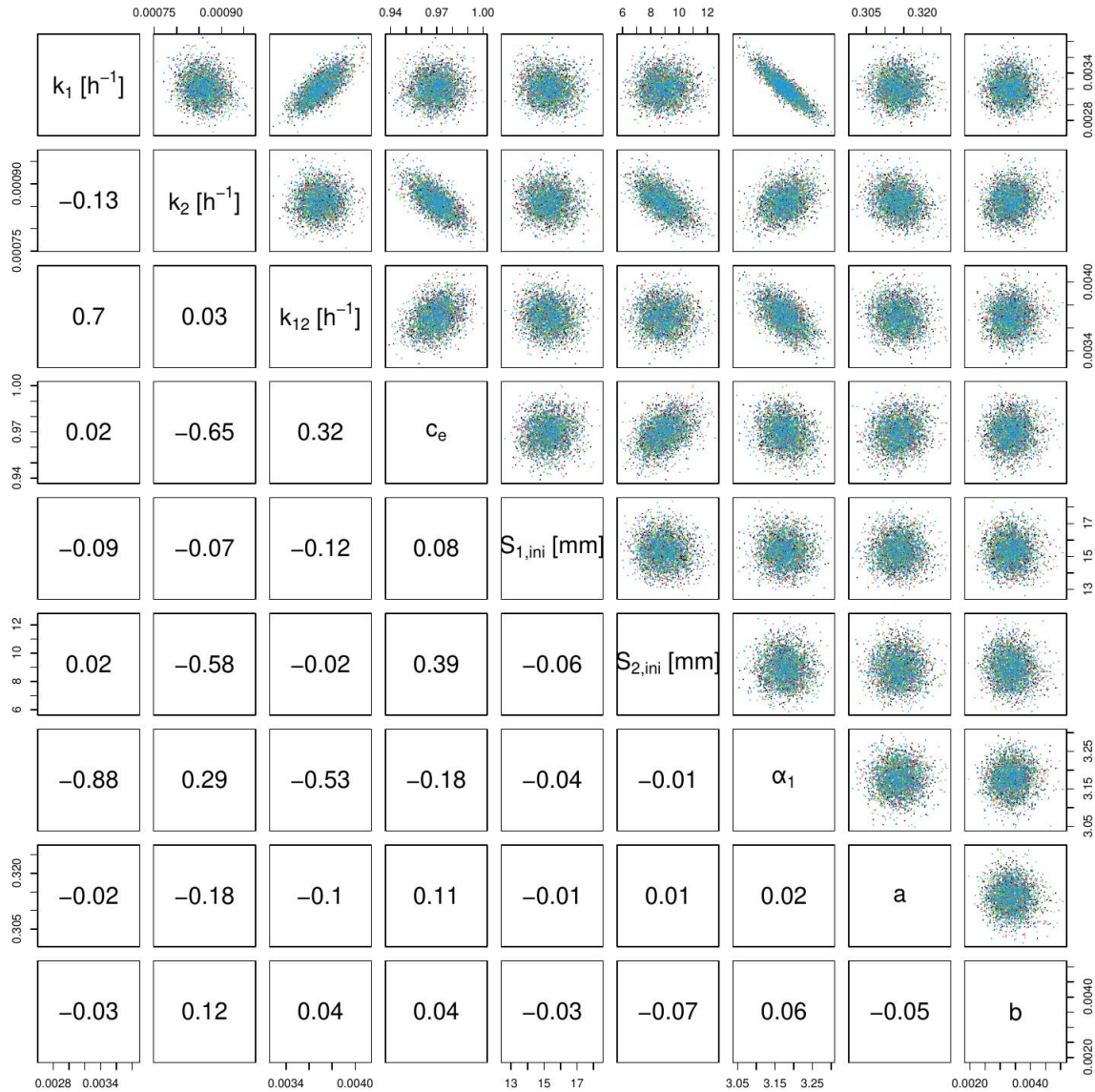


Figure S9. Samples of the two-dimensional posterior marginals of the parameters of model M2b without time-dependent parameters.

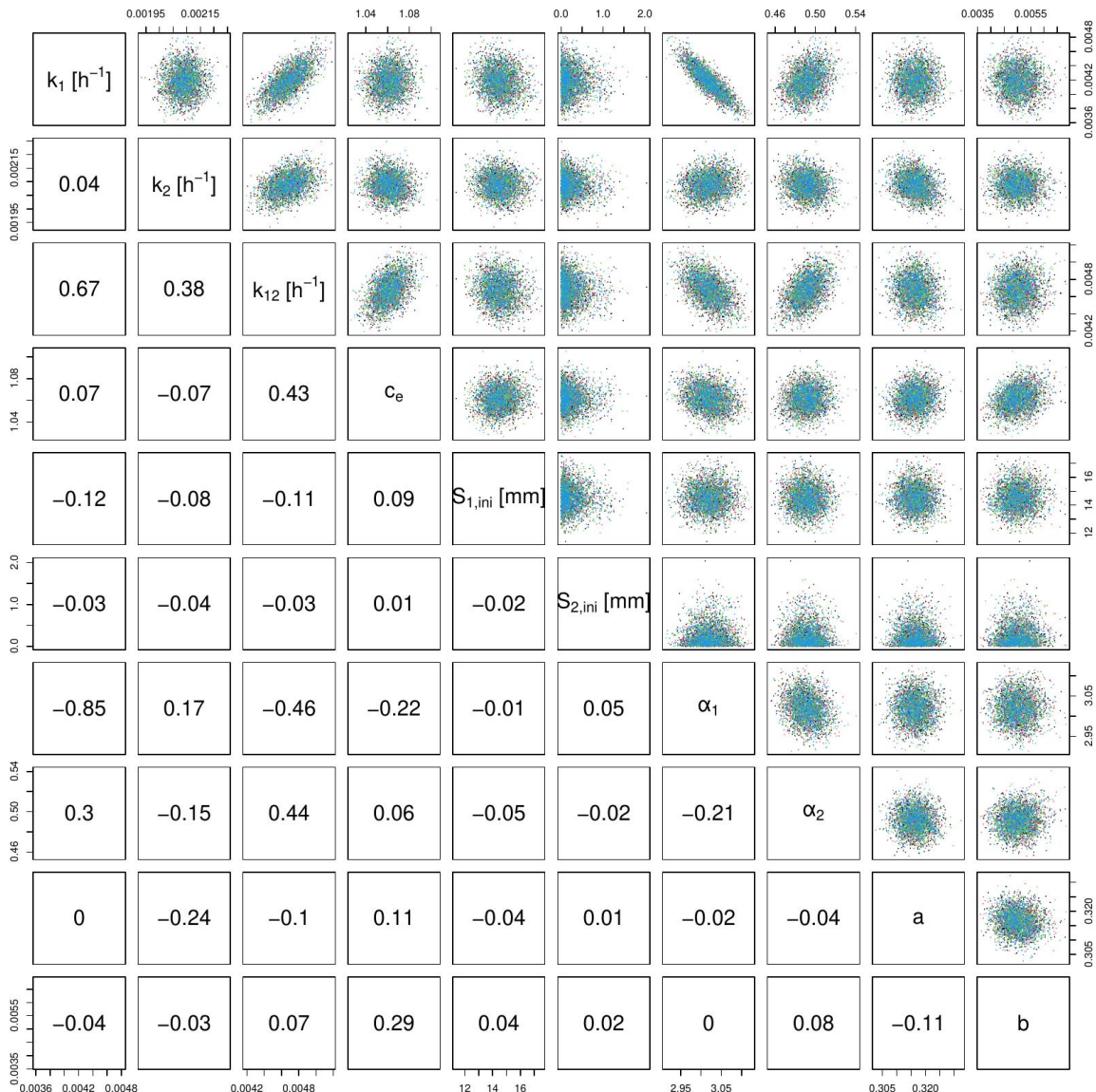


Figure S10. Samples of the two-dimensional posterior marginals of the parameters of model M2c without time-dependent parameters.

Text S3. Time series of discharge and states of the models without time-dependent parameters

The Figures S11 to S15 show the posterior distributions of discharge and state for each of the models M1a, M1b, M2a, M2b and M2c over the full calibration and validation time ranges.

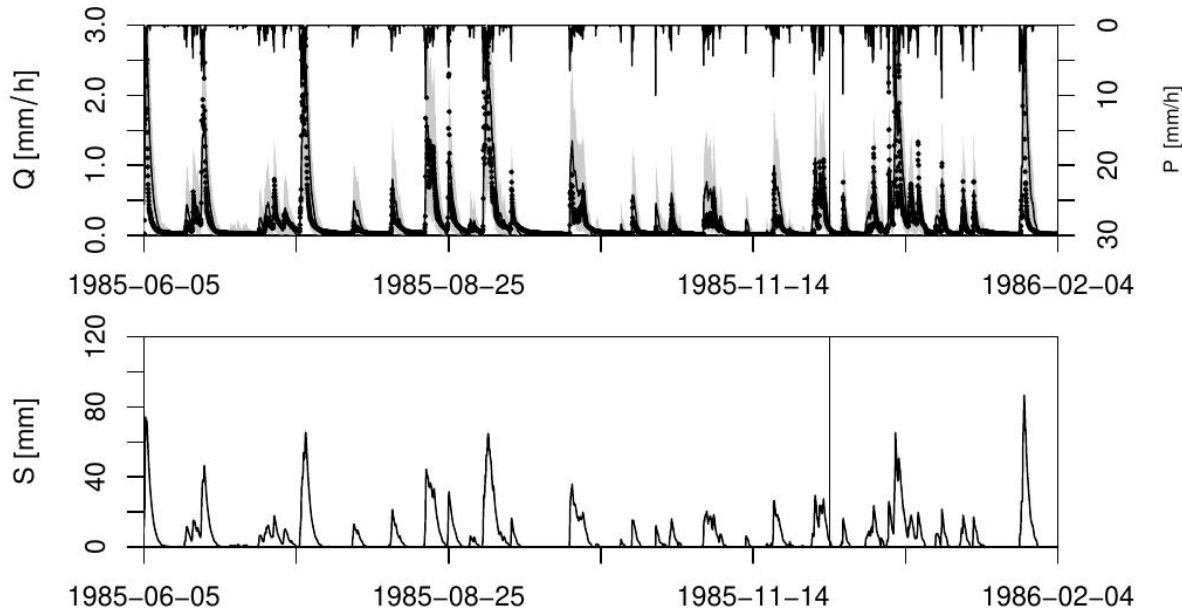


Figure S11. Posterior distribution of discharge and reservoir water level for model M1a without time-dependent parameters over the full calibration and validation time ranges.

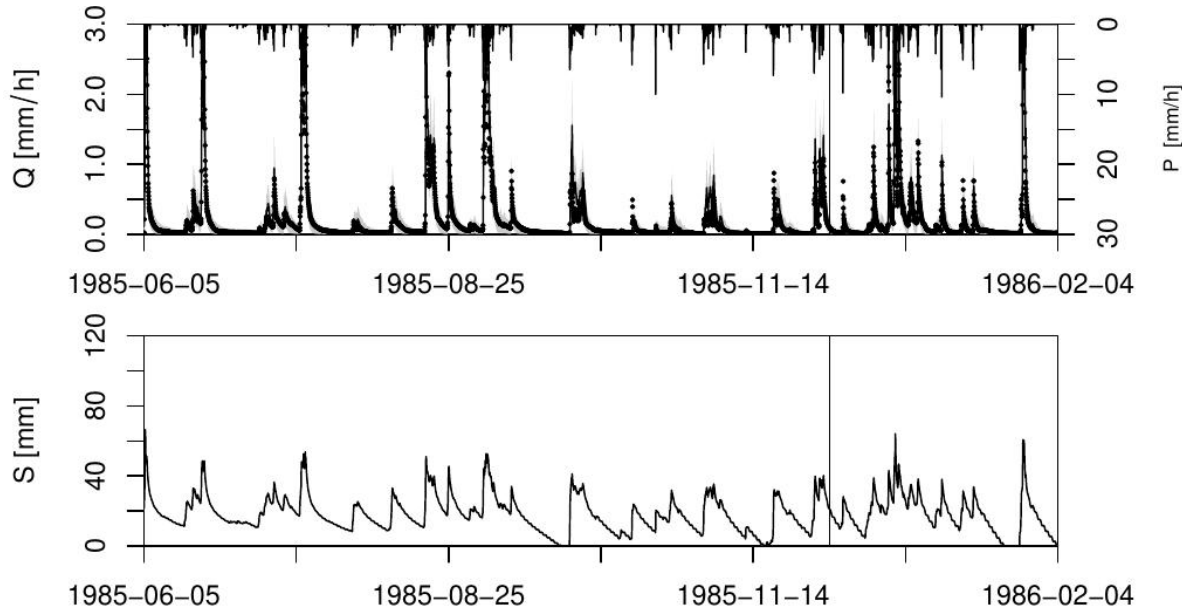


Figure S12. Posterior distribution of discharge and reservoir water level for model M1b without time-dependent parameters over the full calibration and validation time ranges.

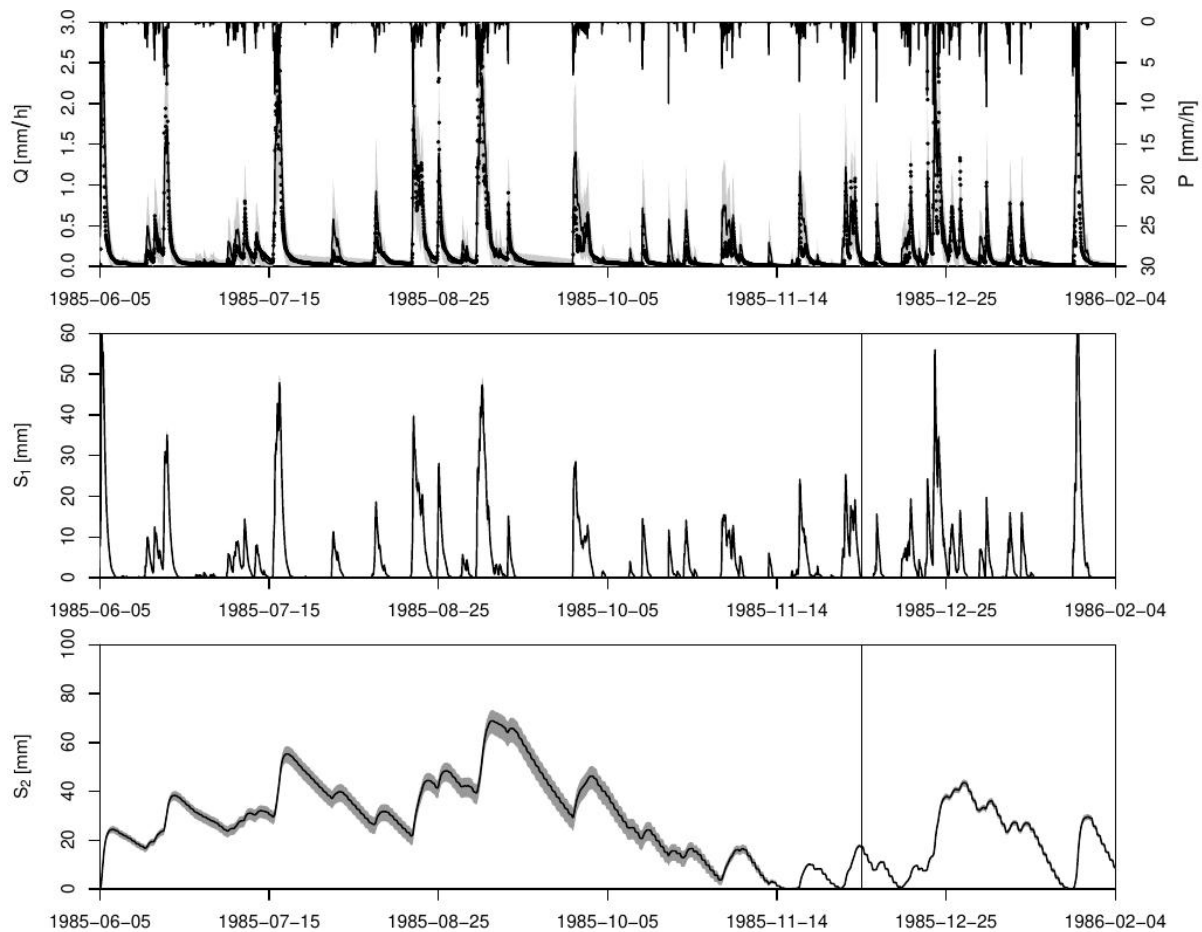


Figure S13. Posterior distribution of discharge and reservoir water levels for model M2a without time-dependent parameters over the full calibration and validation time ranges.

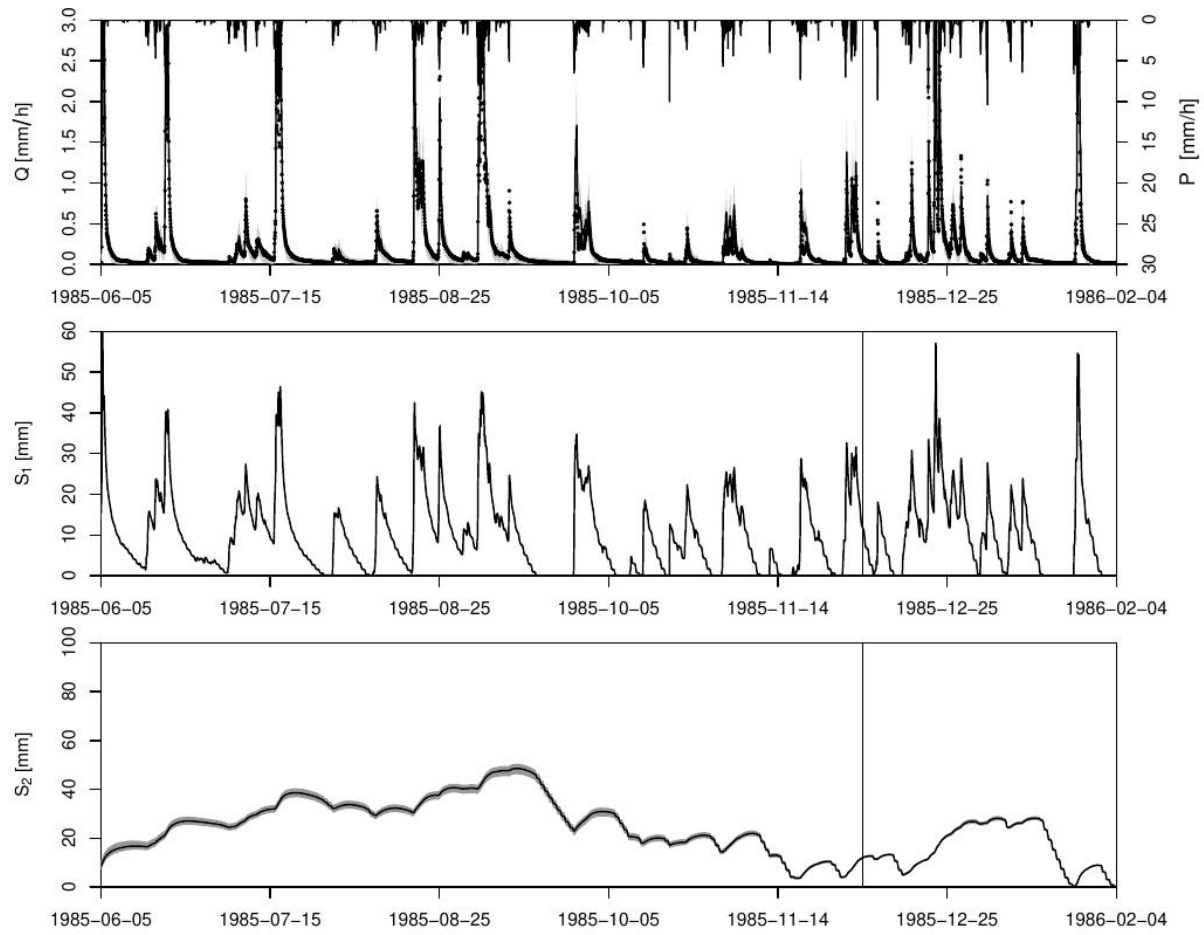


Figure S14. Posterior distribution of discharge and reservoir water levels for model M2b without time-dependent parameters over the full calibration and validation time ranges.

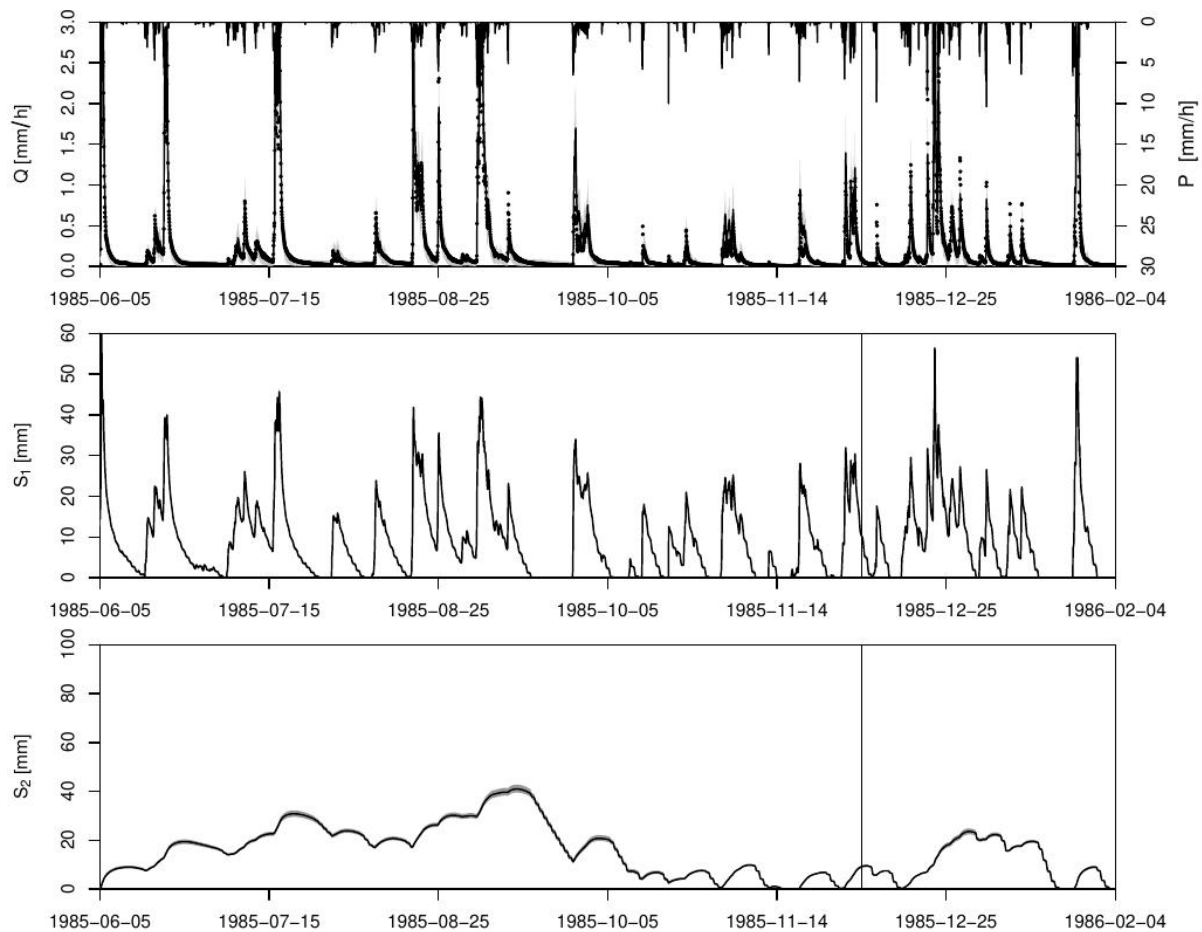


Figure S15. Posterior distribution of discharge and reservoir water levels for model M2c without time-dependent parameters over the full calibration and validation time ranges.

The Figures S16 to S20 show the posterior distributions and three realizations of discharge and state for each of the models M1a, M1b, M2a, M2b and M2c over the final part of the calibration time range and the first part of the validation time range.

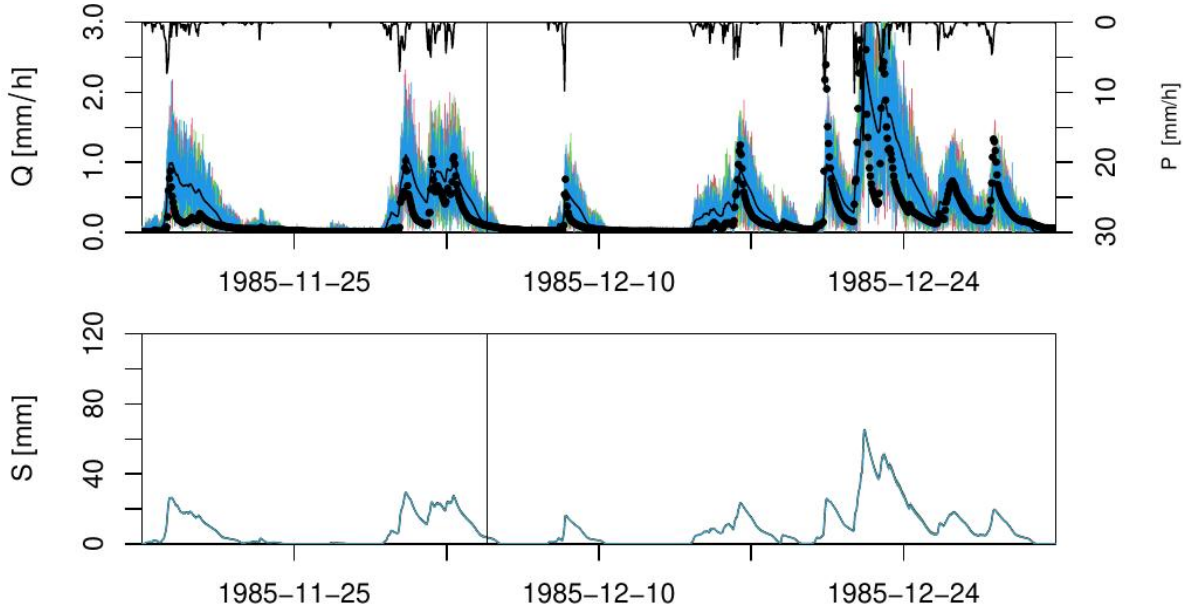


Figure S16. Posterior distribution of discharge and reservoir water level and three realizations of model M1a without time-dependent parameters over the final part of the calibration time range and the first part of the validation time range.

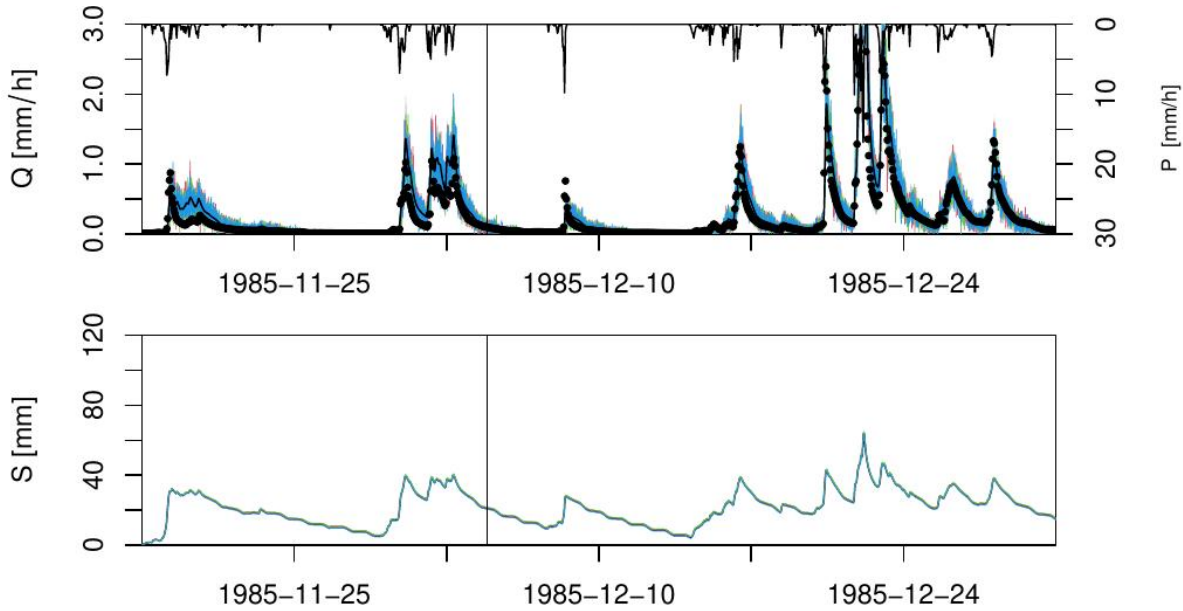


Figure S17. Posterior distribution of discharge and reservoir water level and three realizations of model M1b without time-dependent parameters over the final part of the calibration time range and the first part of the validation time range.

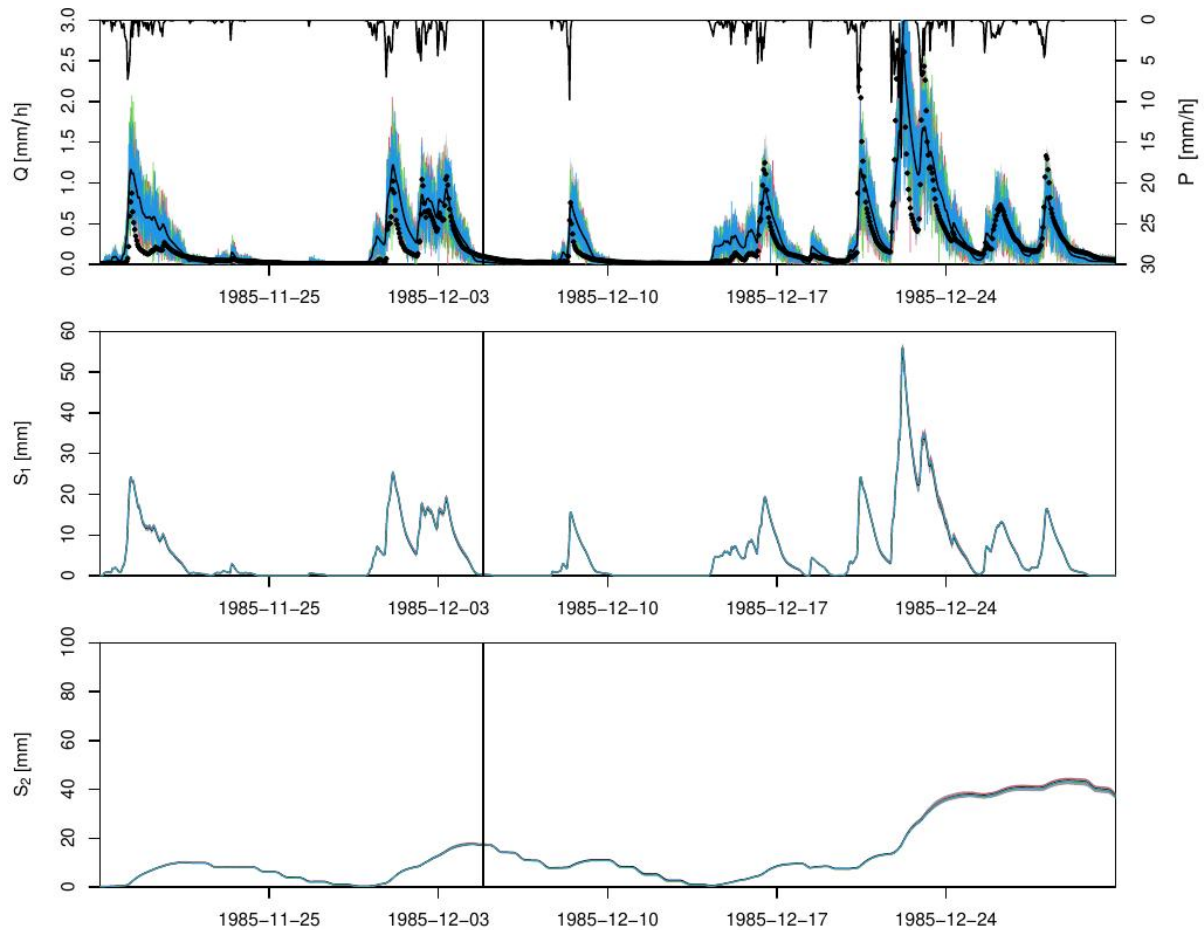


Figure S18. Posterior distribution of discharge and reservoir water levels and three realizations of model M2a without time-dependent parameters over the final part of the calibration time range and the first part of the validation time range.

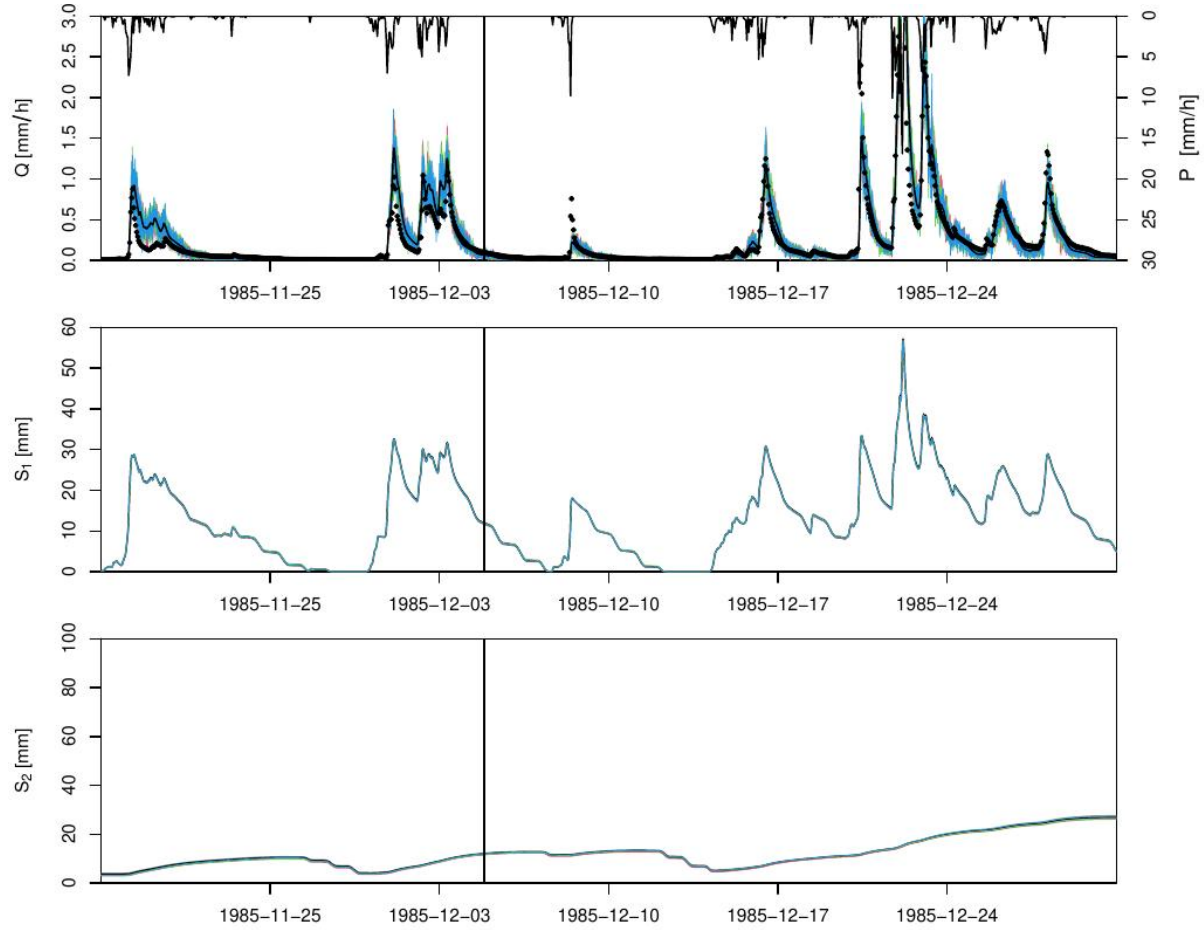


Figure S19. Posterior distribution of discharge and reservoir water levels and three realizations of model M2b without time-dependent parameters over the final part of the calibration time range and the first part of the validation time range.

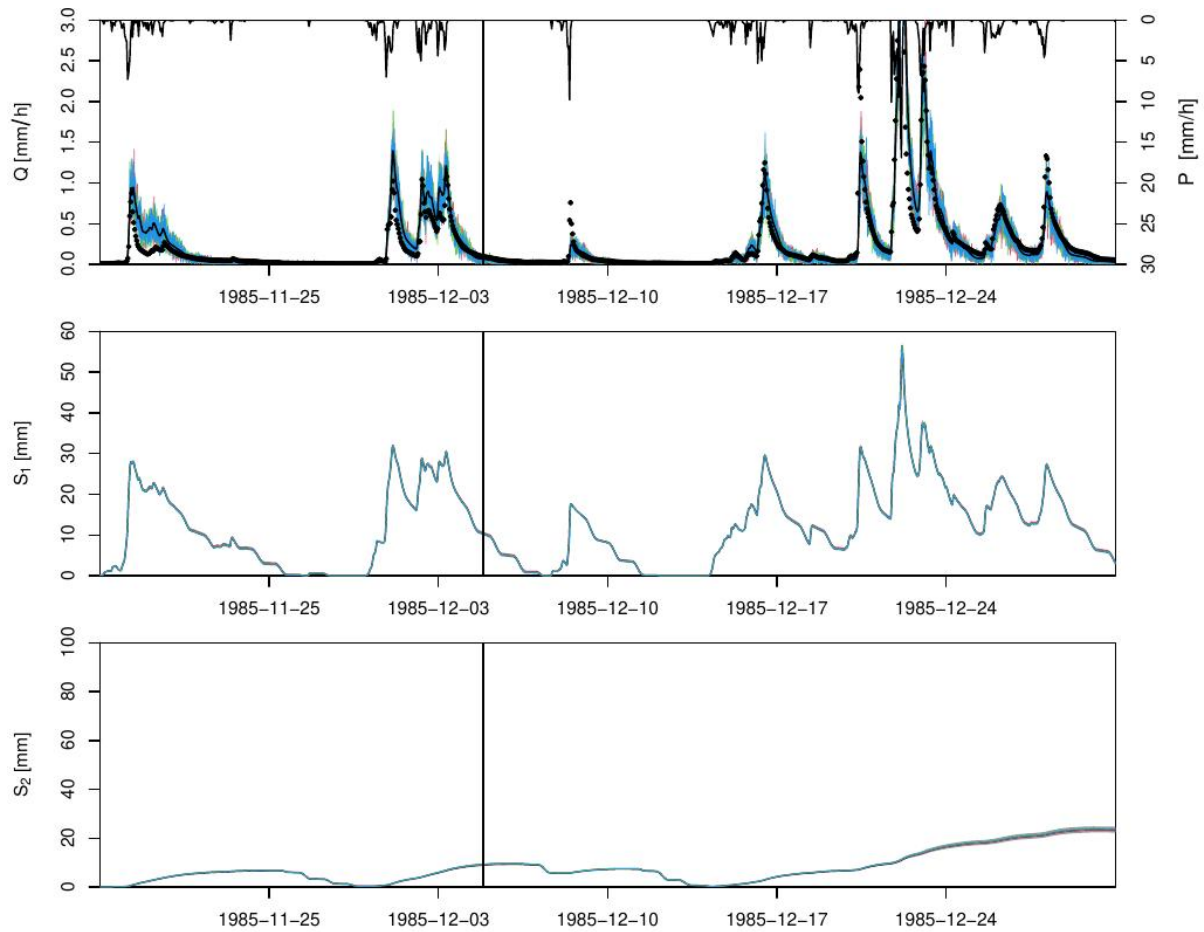


Figure S20. Posterior distribution of discharge and reservoir water levels and three realizations of model M2c without time-dependent parameters over the final part of the calibration time range and the first part of the validation time range.

The Figures S21 to S25 show the posterior distributions and three realizations of discharge and state for each of the models M1a, M1b, M2a, M2b and M2c over a small part of the validation time range.

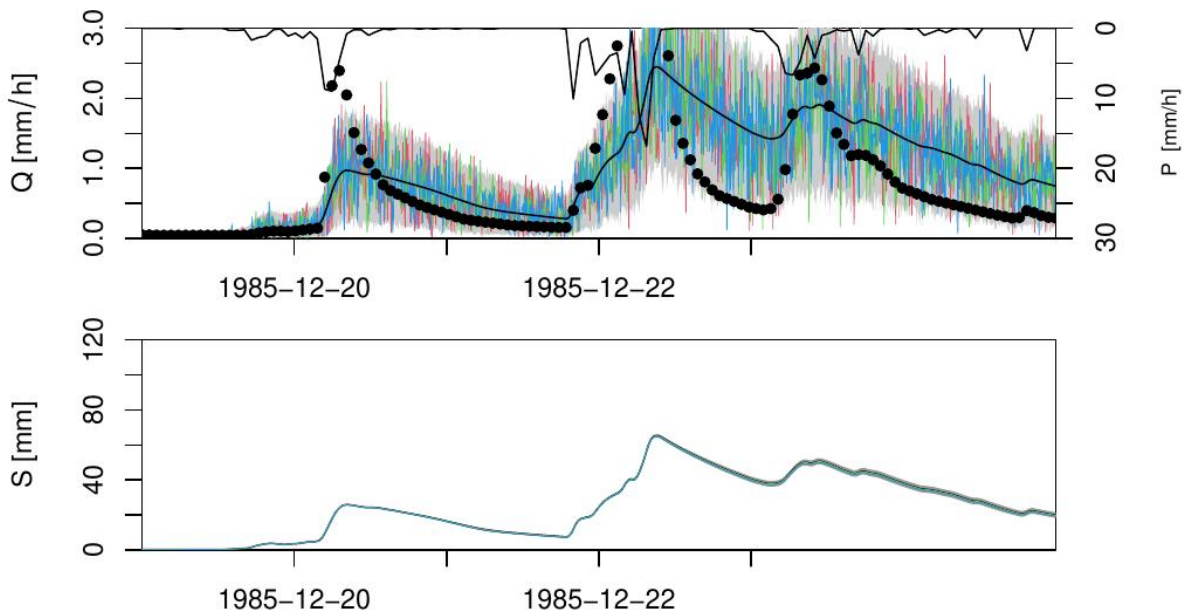


Figure S21. Posterior distribution of discharge and reservoir water level and three realizations of model M1a without time-dependent parameters over a small part of the validation time range.

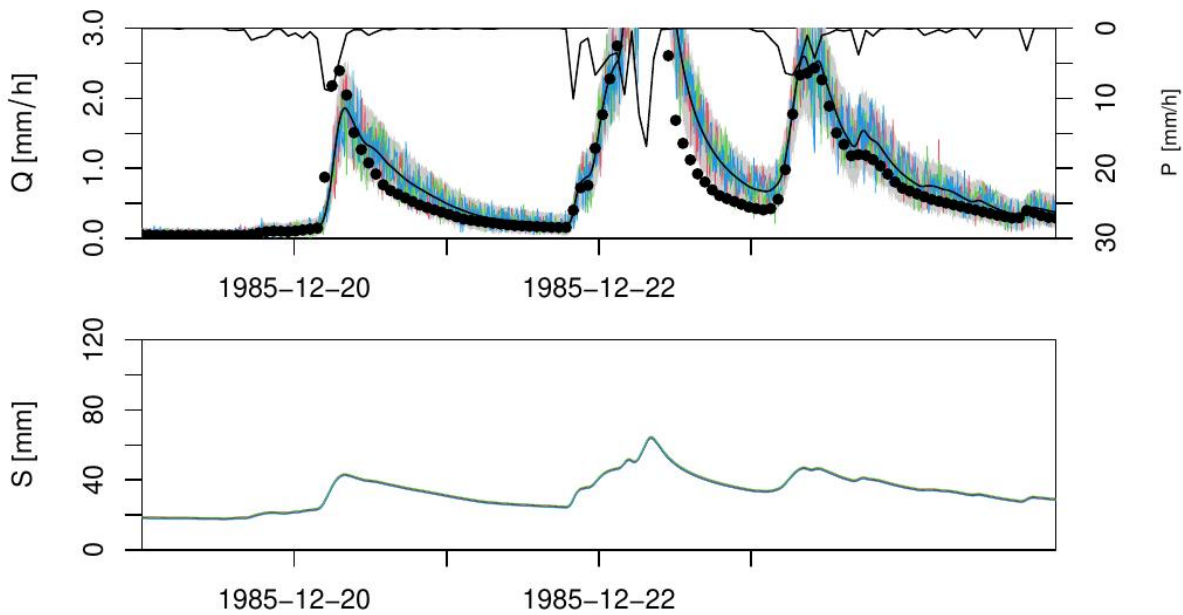


Figure S22. Posterior distribution of discharge and reservoir water level and three realizations of model M1b without time-dependent parameters over a small part of the validation time range.

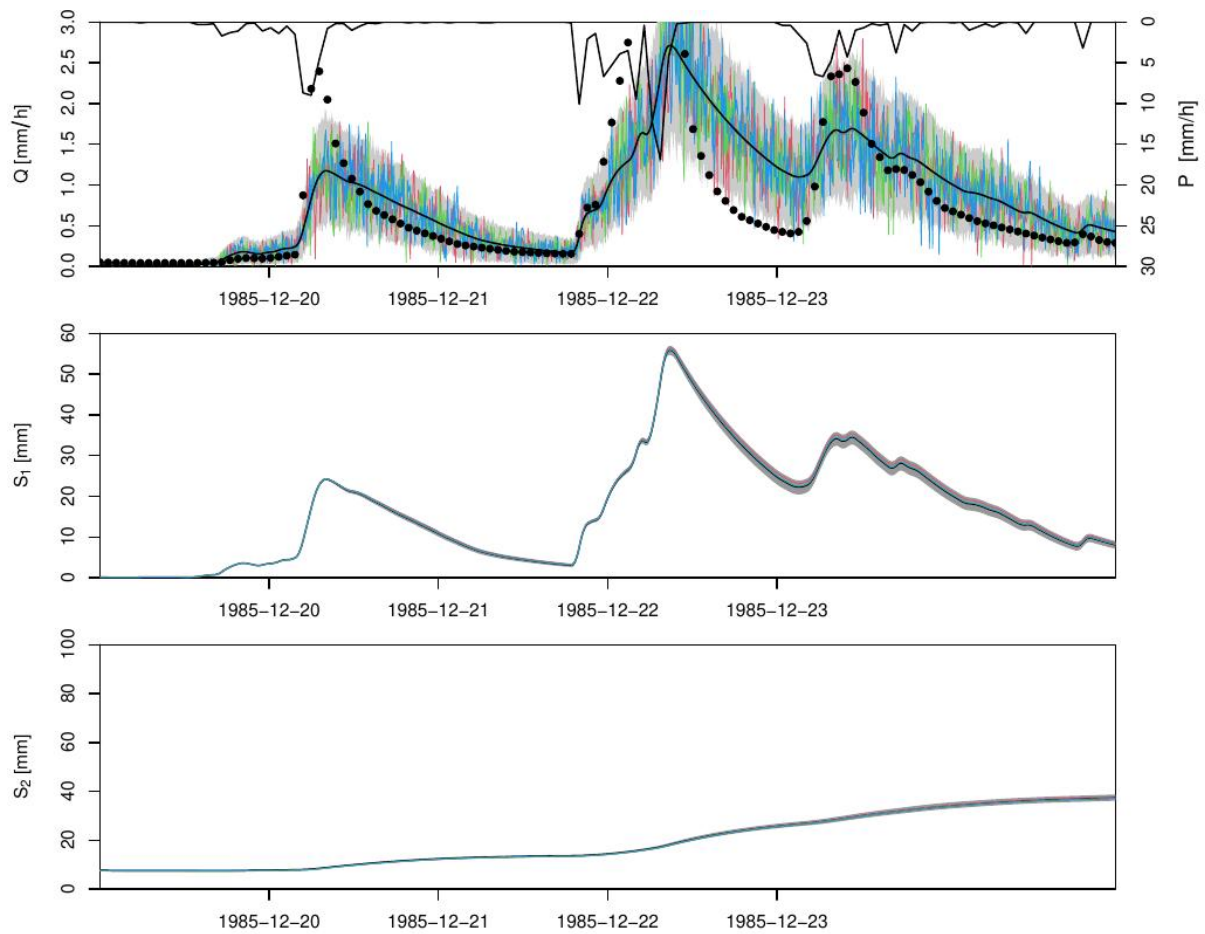


Figure S23. Posterior distribution of discharge and reservoir water levels and three realizations of model M2a without time-dependent parameters over a small part of the validation time range.

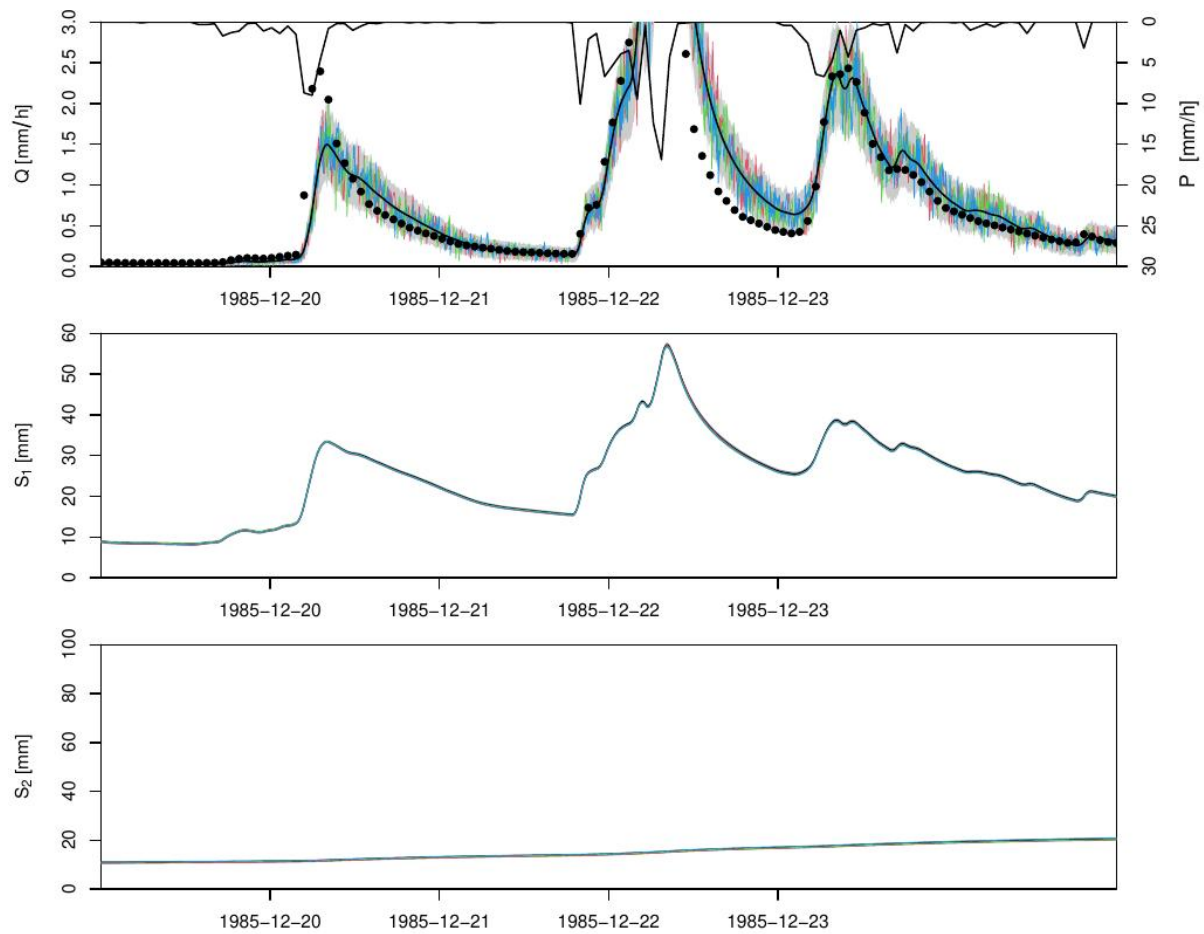


Figure S24. Posterior distribution of discharge and reservoir water levels and three realizations of model M2b without time-dependent parameters over a small part of the validation time range.

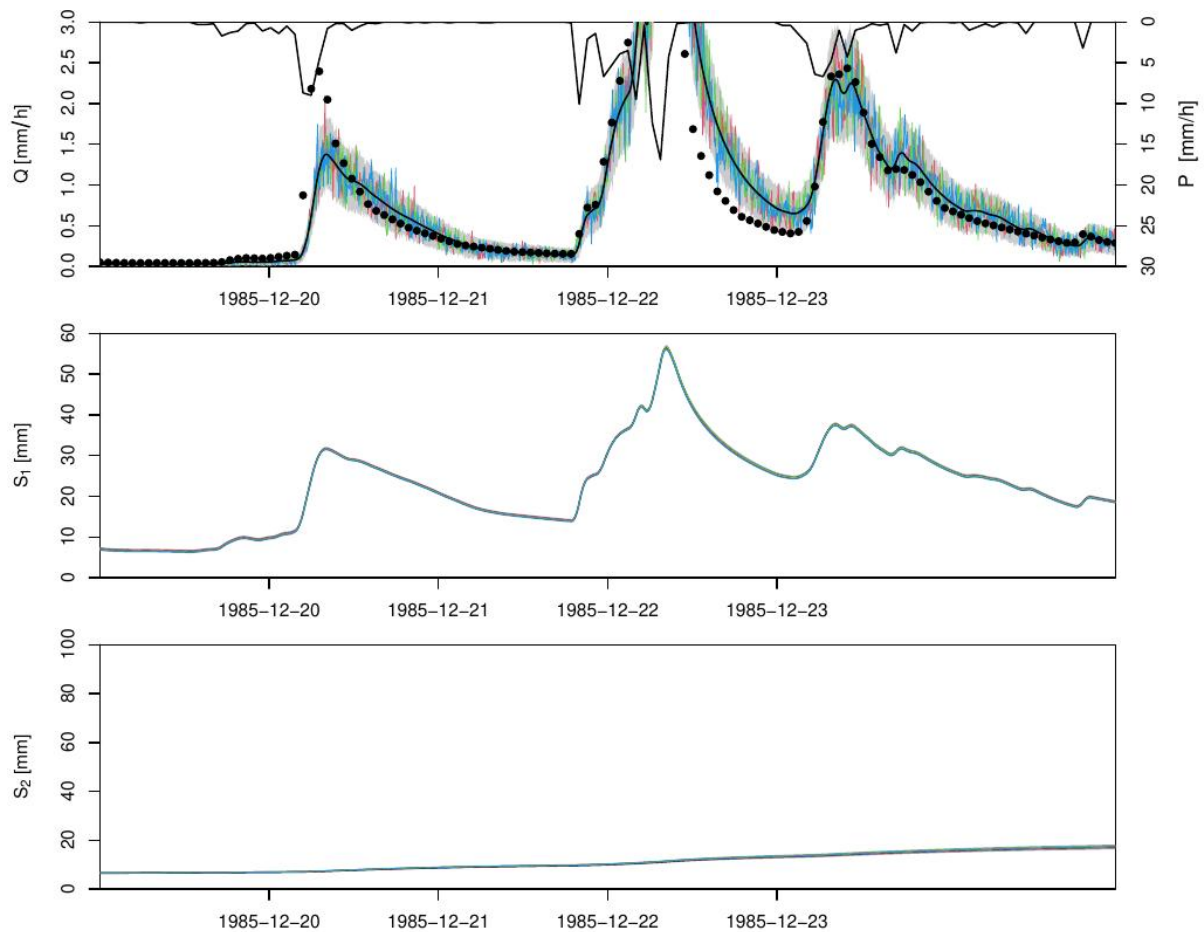


Figure S25. Posterior distribution of discharge and reservoir water levels and three realizations of model M2c without time-dependent parameters over a small part of the validation time range.

Text S4. Markov chains and one-dimensional marginal posterior distributions of constant and Ornstein-Uhlenbeck parameters

The Figures S26 to S30 show four Markov chains of the constant and Ornstein-Uhlenbeck parameters of each of the models M1a, M1b, M2a, M2b and M2c with time-dependent parameters. Each figure shows the 1d projections of the four chains (left) and the corresponding marginal densities (right). The Markov chains were started from previous burn-in runs. The red line indicates the end of the adaptation phase of the Metropolis algorithm, the blue, dashed line marks the iteration at which the evaluation of the chain starts (to be sure not to have remaining burn-in in the evaluation).

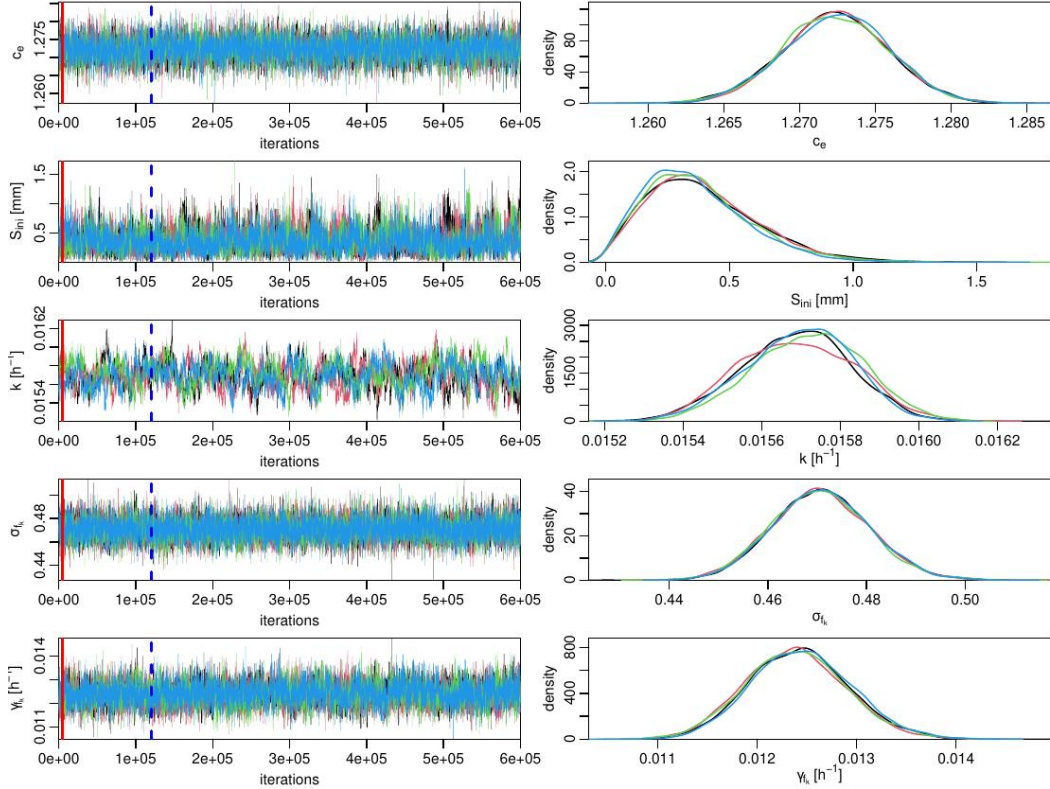


Figure S26. Markov chains and one-dimensional posterior marginals of constant and Ornstein-Uhlenbeck parameters for model M1a with time-dependent parameter f_k .

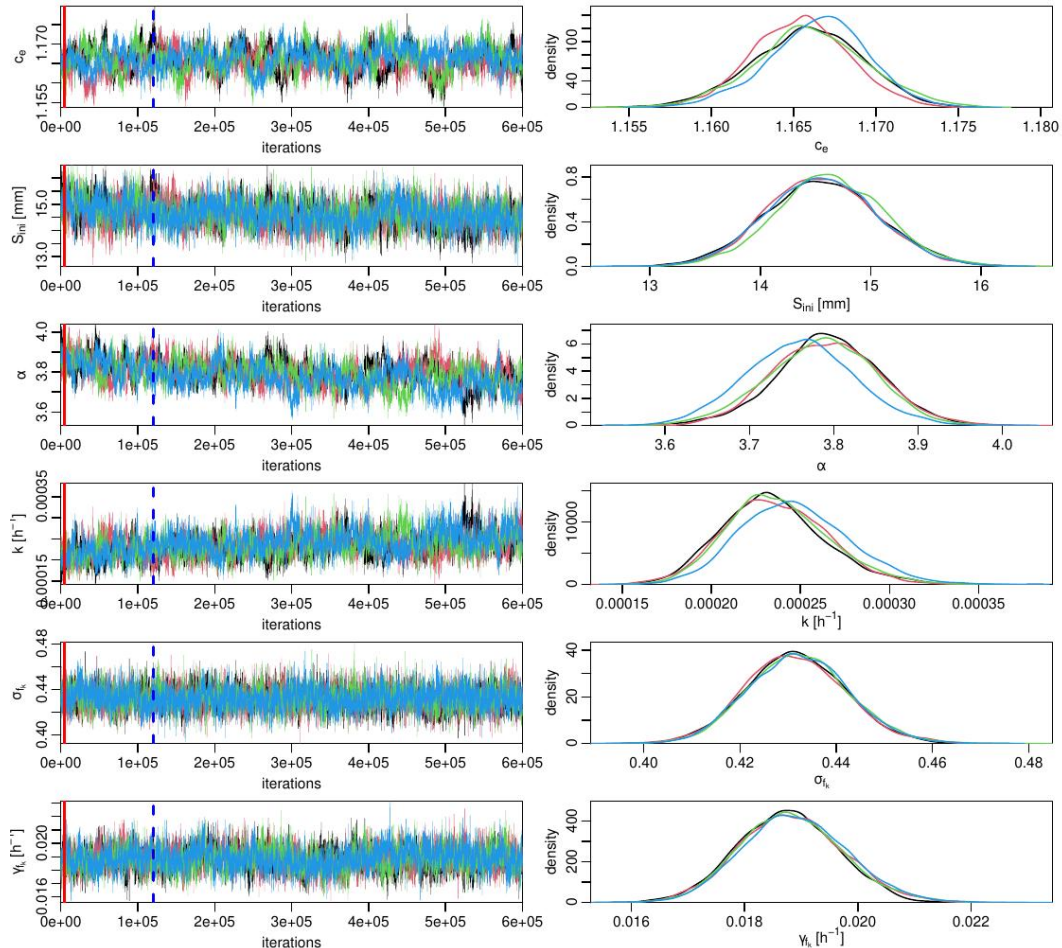


Figure S27. Markov chains and one-dimensional posterior marginals of constant and Ornstein-Uhlenbeck parameters for model M1b with time-dependent parameter f_k .

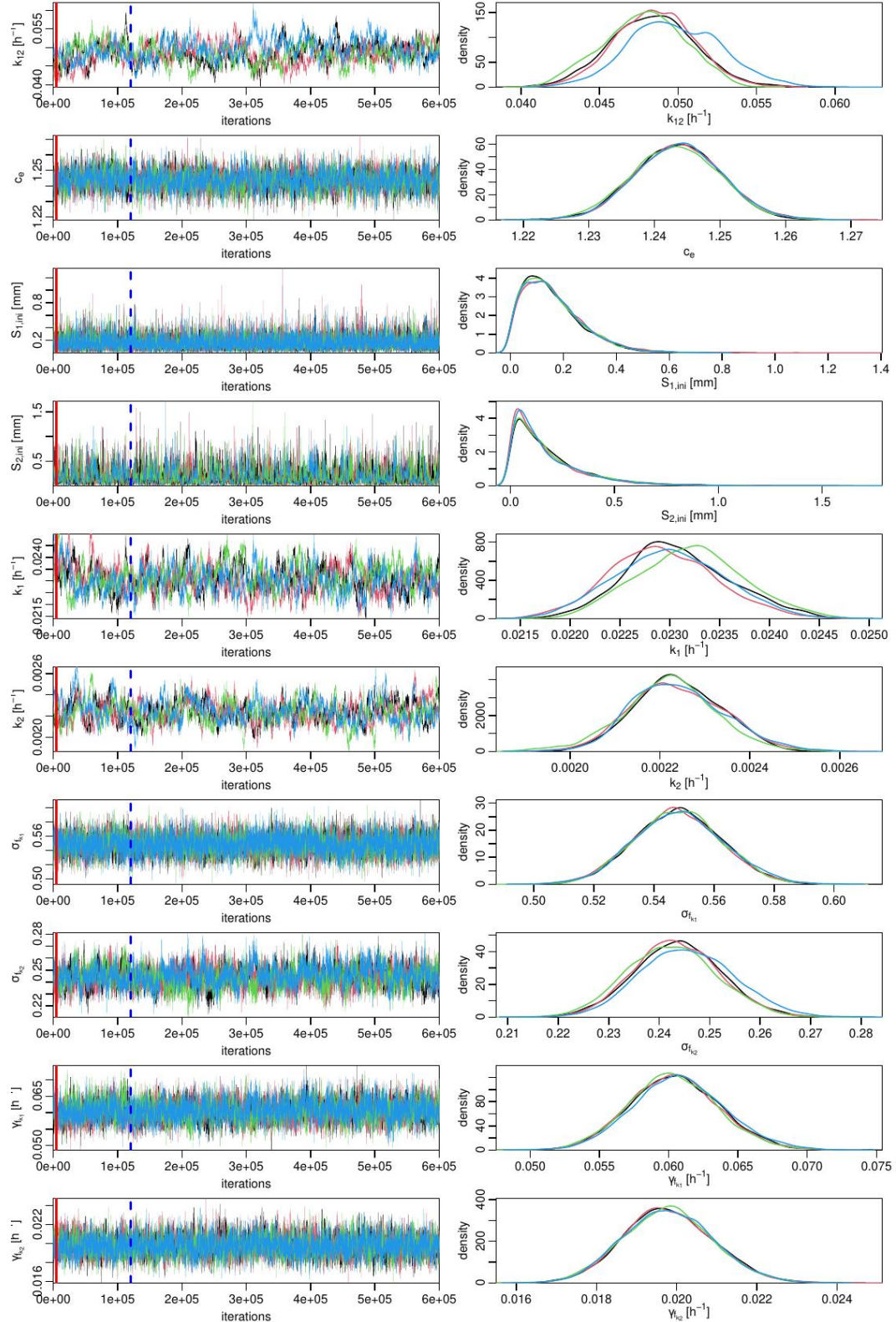


Figure S28. Markov chains and one-dimensional posterior marginals of constant and Ornstein-Uhlenbeck parameters for model M2a with time-dependent parameters f_{k_1} and f_{k_2} .

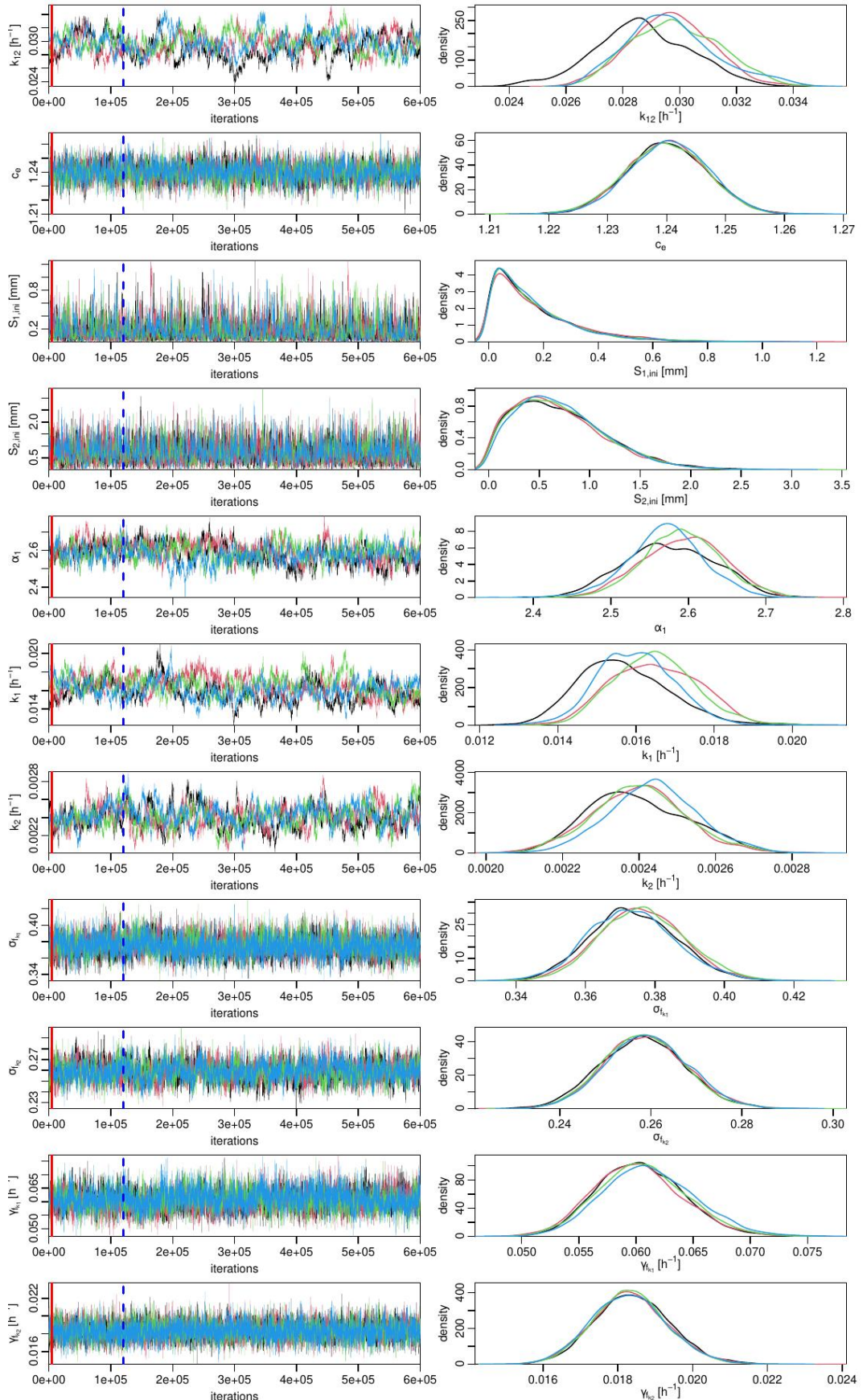


Figure S29. Markov chains and one-dimensional posterior marginals of constant and Ornstein-Uhlenbeck parameters for model M2b with time-dependent parameters f_{k_1} and f_{k_2} .

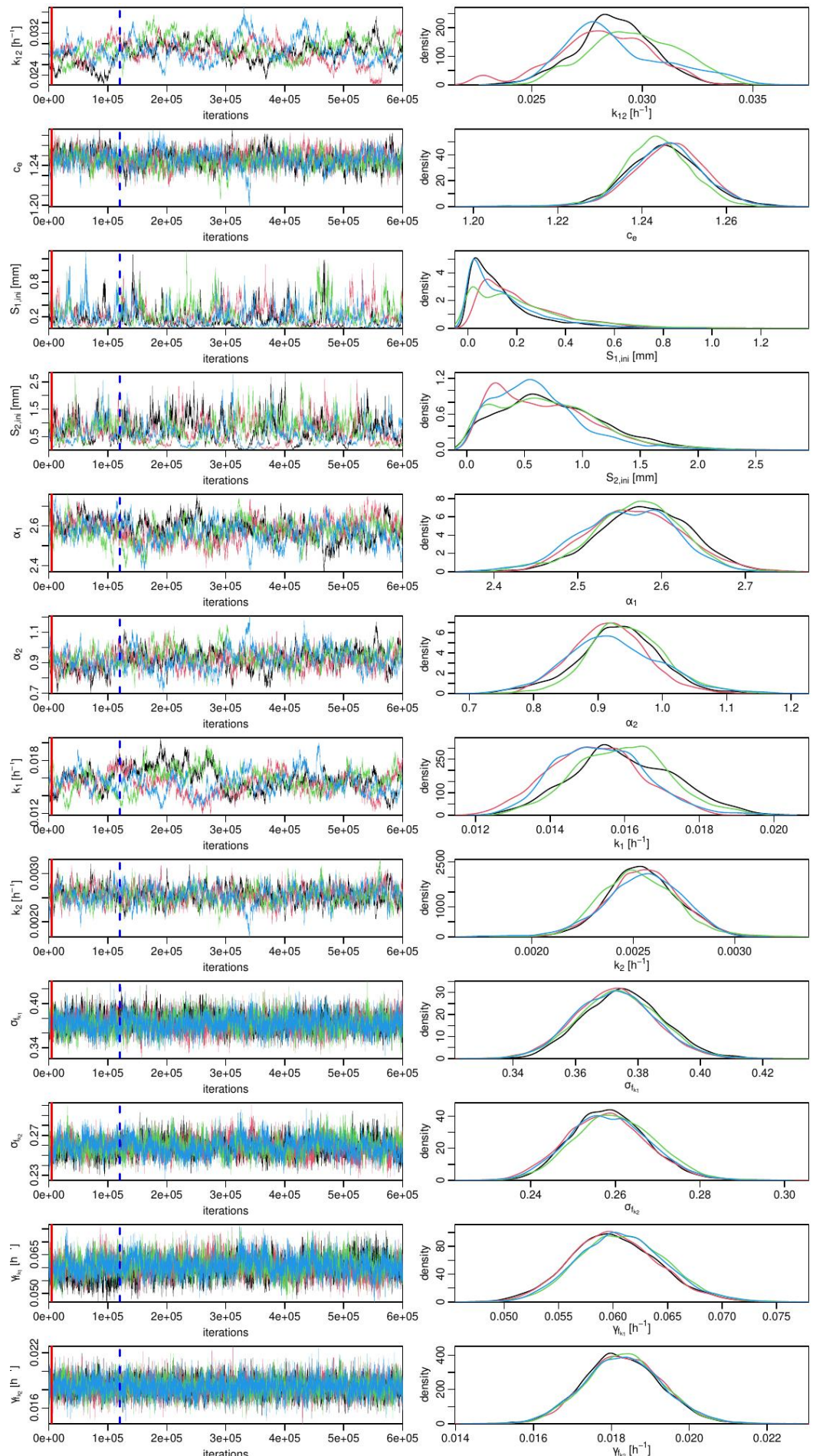


Figure S30. Markov chains and one-dimensional posterior marginals of constant and Ornstein-Uhlenbeck parameters for model M2c with time-dependent parameters f_{k_1} and f_{k_2} .

Text S5. Two-dimensional marginal posterior distributions of constant and Ornstein-Uhlenbeck parameters

The Figures S31 to S35 show samples of two-dimensional posterior marginals of constant and Ornstein-Uhlenbeck parameters of four Markov chains for each of the models M1a, M1b, M2a, M2b and M2c with time-dependent parameters.

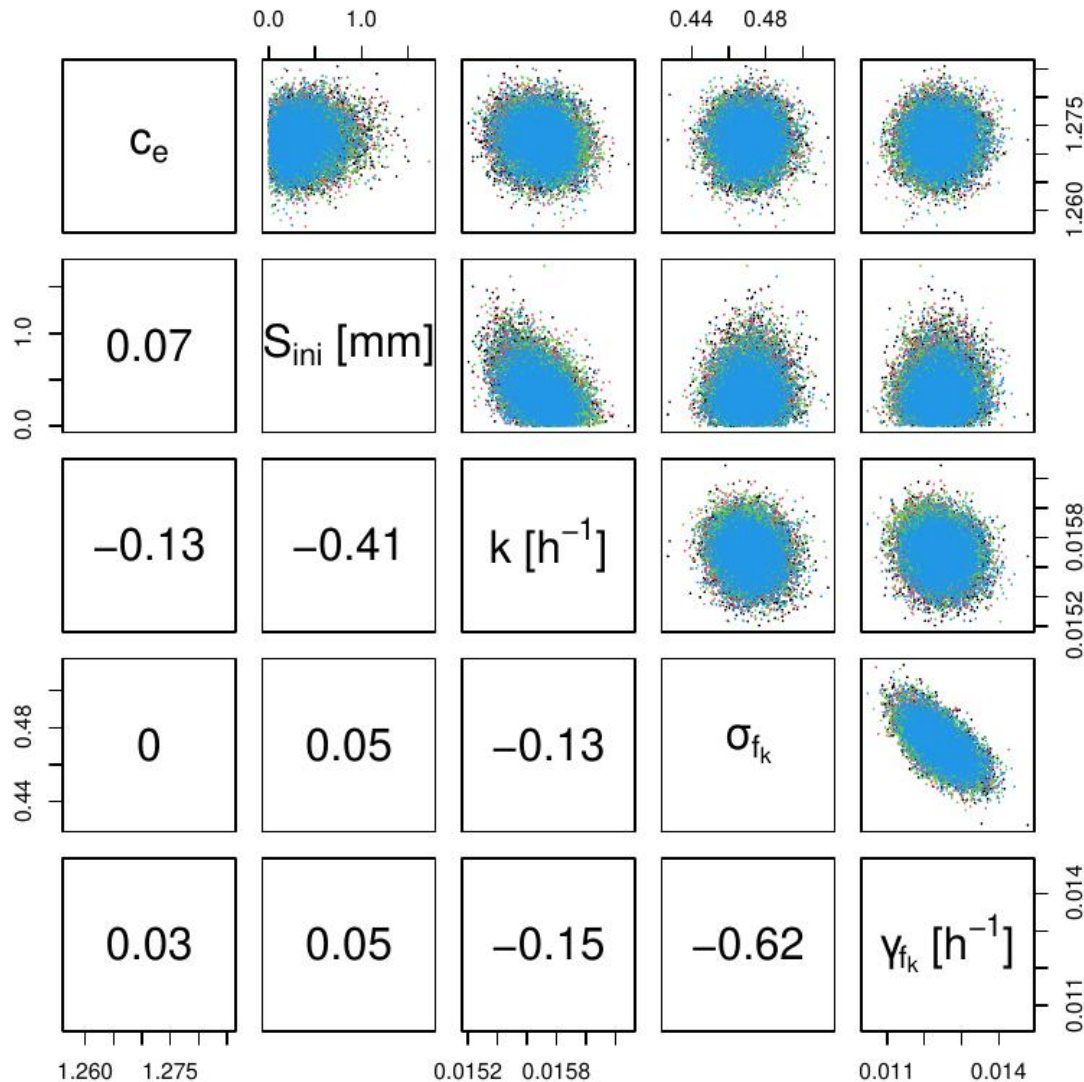


Figure S31. Samples of the two-dimensional posterior marginals of constant and Ornstein-Uhlenbeck parameters for model M1a with time-dependent parameter f_k .

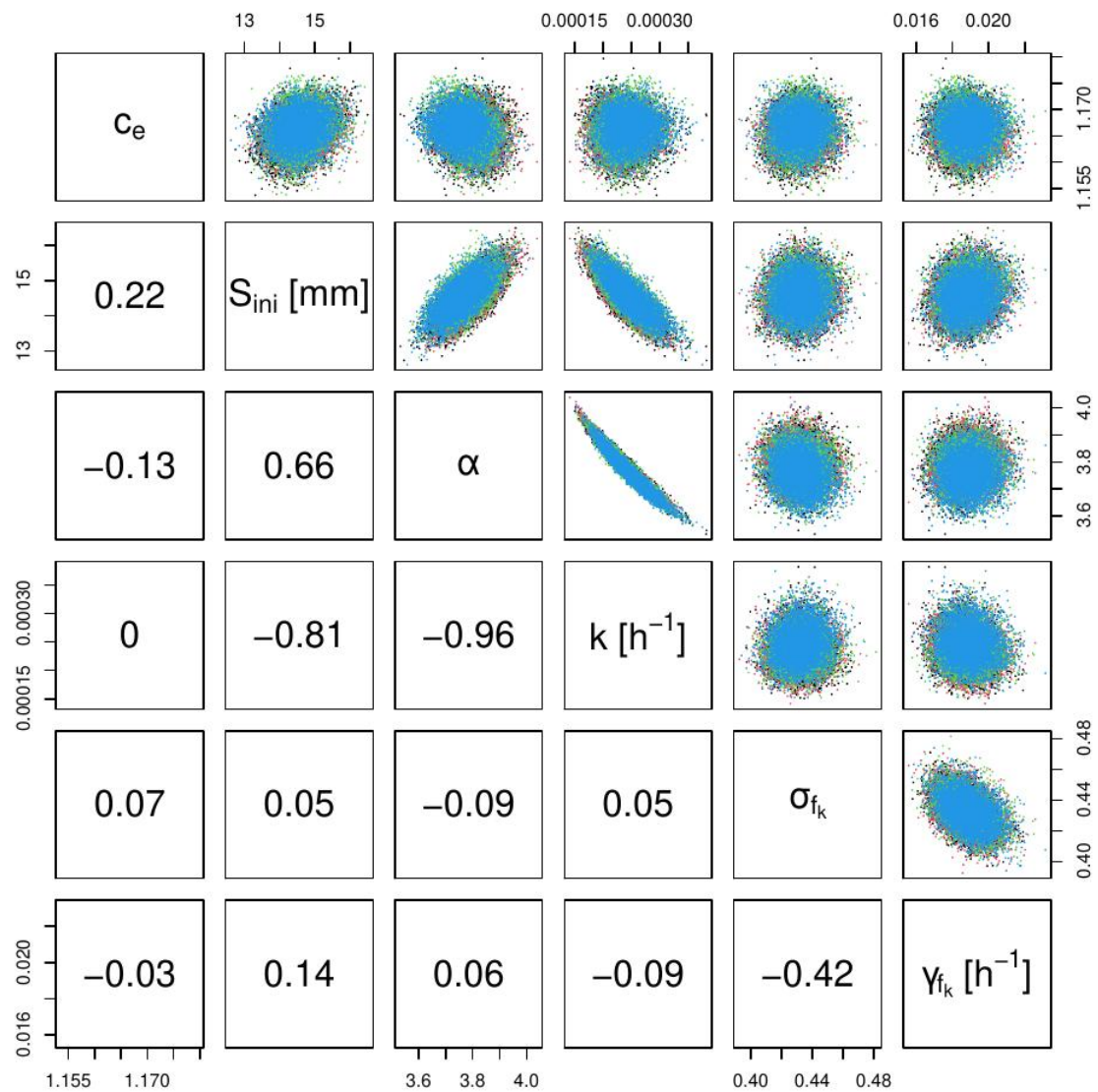


Figure S32. Samples of the two-dimensional posterior marginals of constant and Ornstein-Uhlenbeck parameters for model M1b with time-dependent parameter f_k .

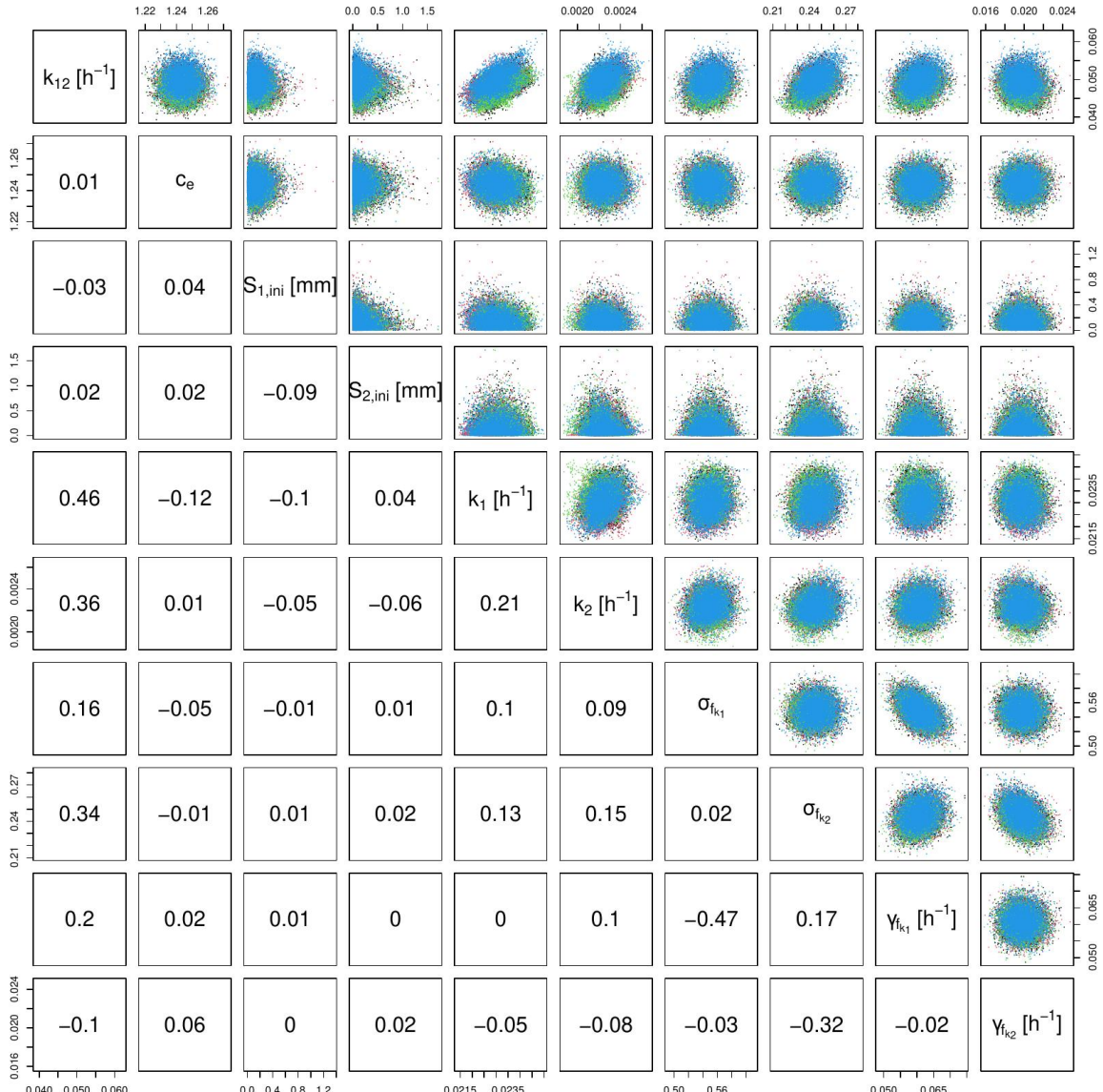


Figure S33. Samples of the two-dimensional posterior marginals of constant and Ornstein-Uhlenbeck parameters for model M2a with time-dependent parameters f_{k_1} and f_{k_2} .

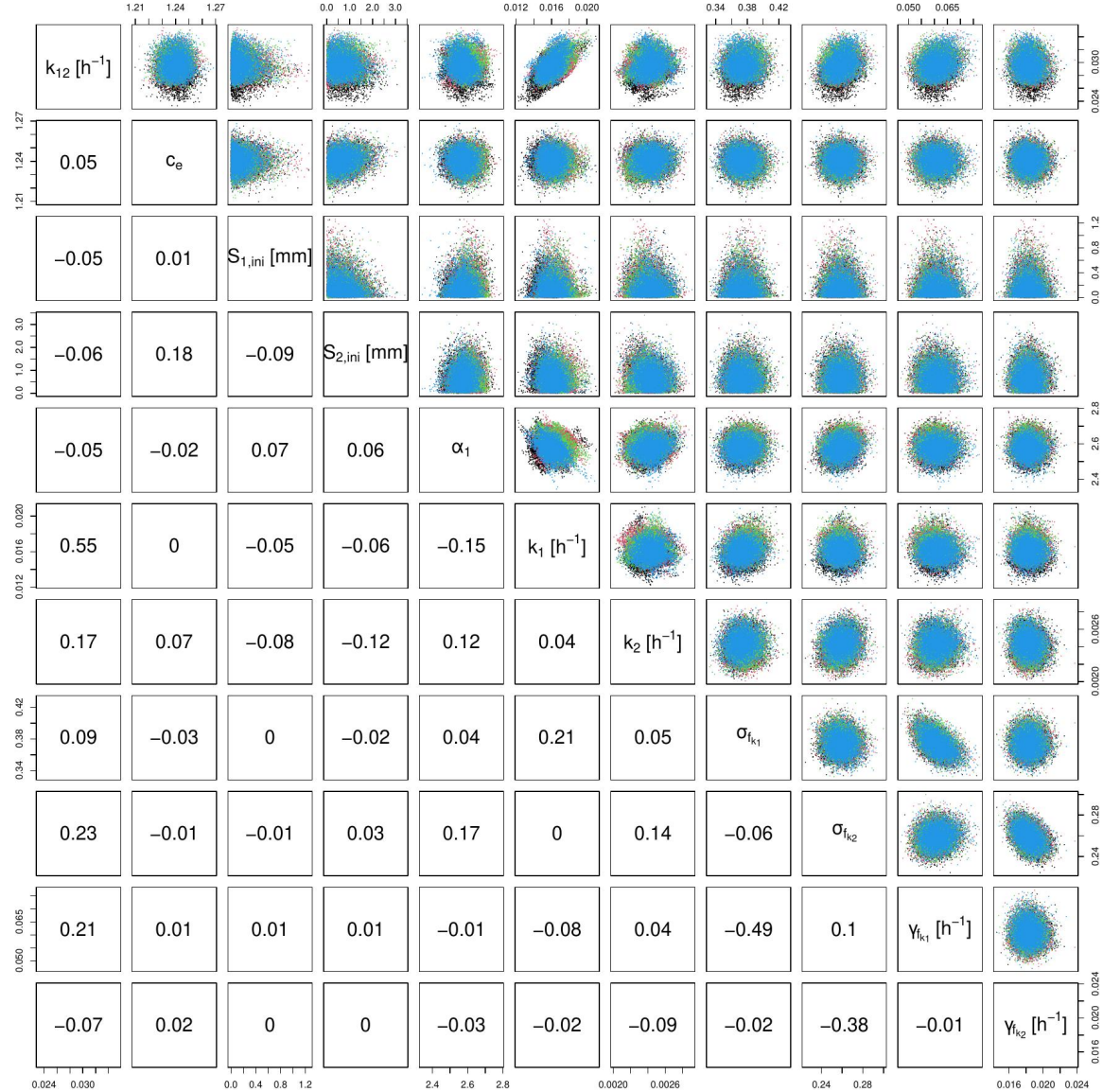


Figure S34. Samples of the two-dimensional posterior marginals of constant and Ornstein-Uhlenbeck parameters for model M2b with time-dependent parameters f_{k_1} and f_{k_2} .

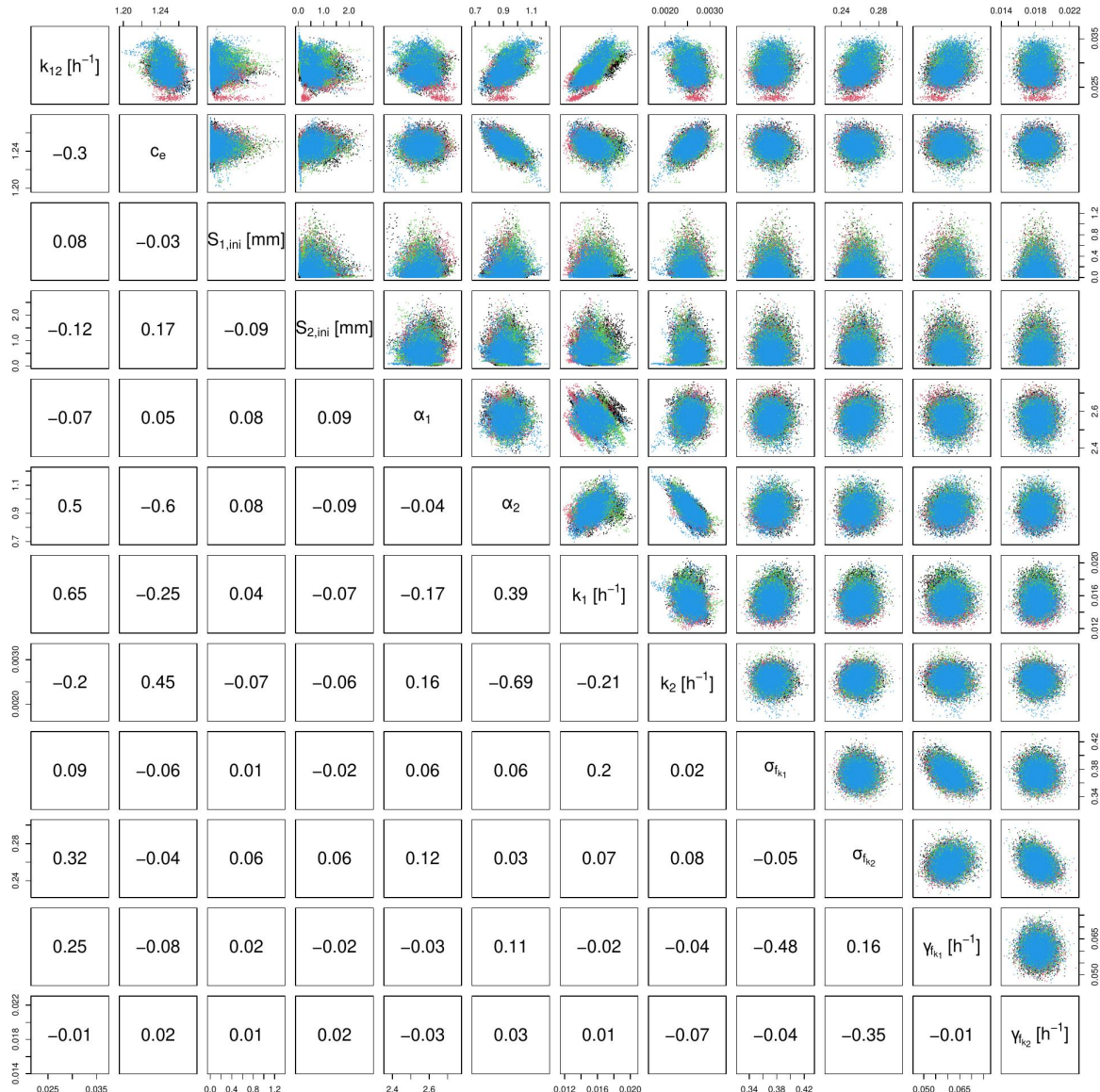


Figure S35. Samples of the two-dimensional posterior marginals of constant and Ornstein-Uhlenbeck parameters for model M2c with time-dependent parameters f_{k_1} and f_{k_2} .

Text S6. Markov chains and one-dimensional marginal posterior distributions of time-dependent parameters at selected time points

The Figures S36 to S43 show four Markov chains for each of the models M1a, M1b, M2a, M2b and M2c with time-dependent parameters. Each figure shows the 1d projections of the four chains (left) and the corresponding marginal densities of the time-dependent parameter(s) at some points in time (right). The Markov chains were started from previous burn-in runs. The red line indicates the end of the adaptation phase of the Metropolis algorithm, the blue, dashed line marks the iteration at which the evaluation of the chain starts (to be sure not to have remaining burn-in in the evaluation).

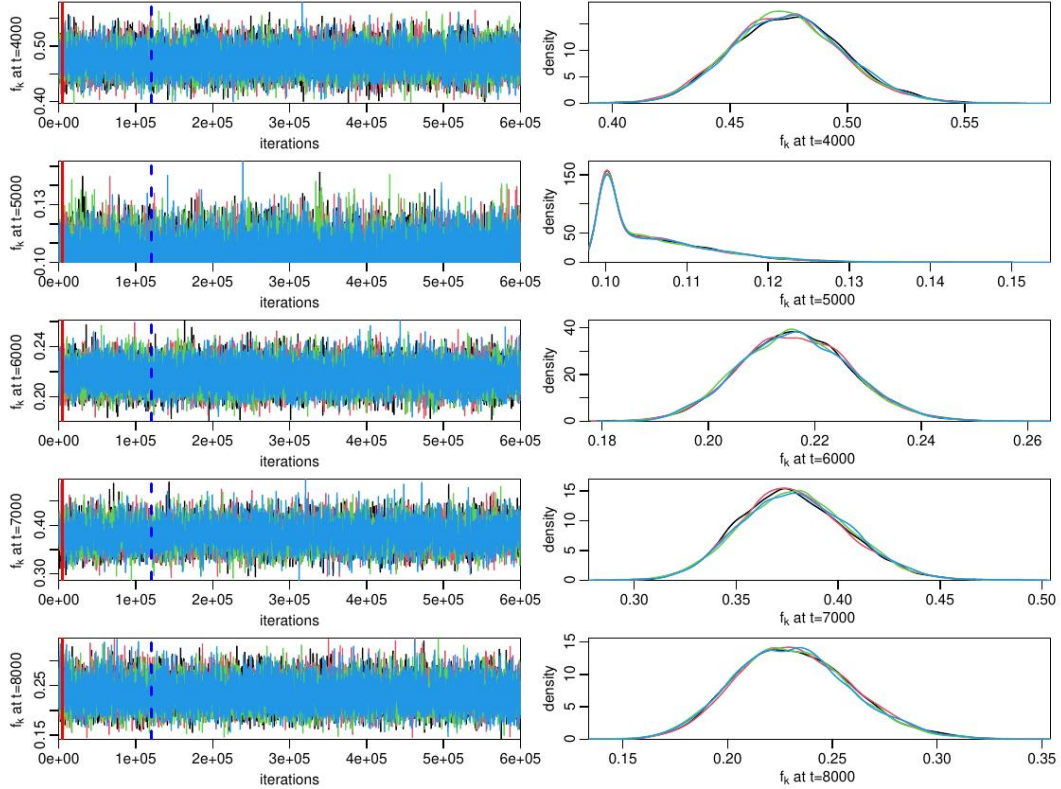


Figure S36. Markov chains and one-dimensional posterior marginals of the time-dependent parameter f_k for model M1a at selected points in time.

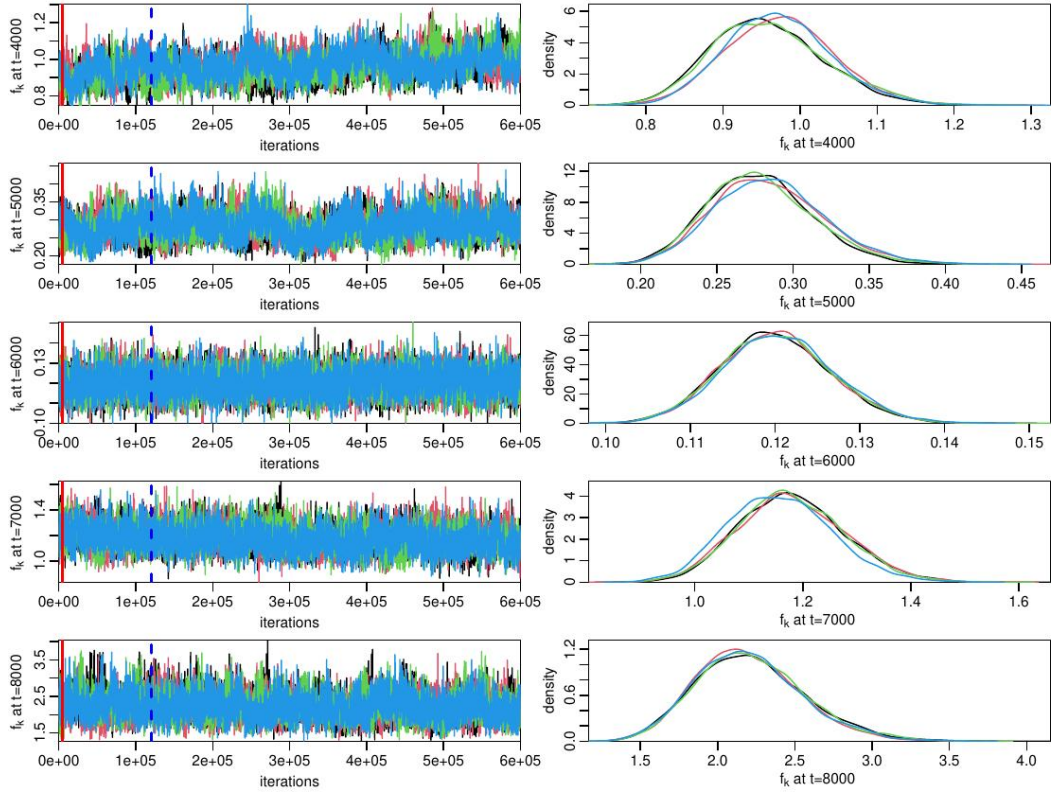


Figure S37. Markov chains and one-dimensional posterior marginals of the time-dependent parameter f_k for model M1b at selected points in time.

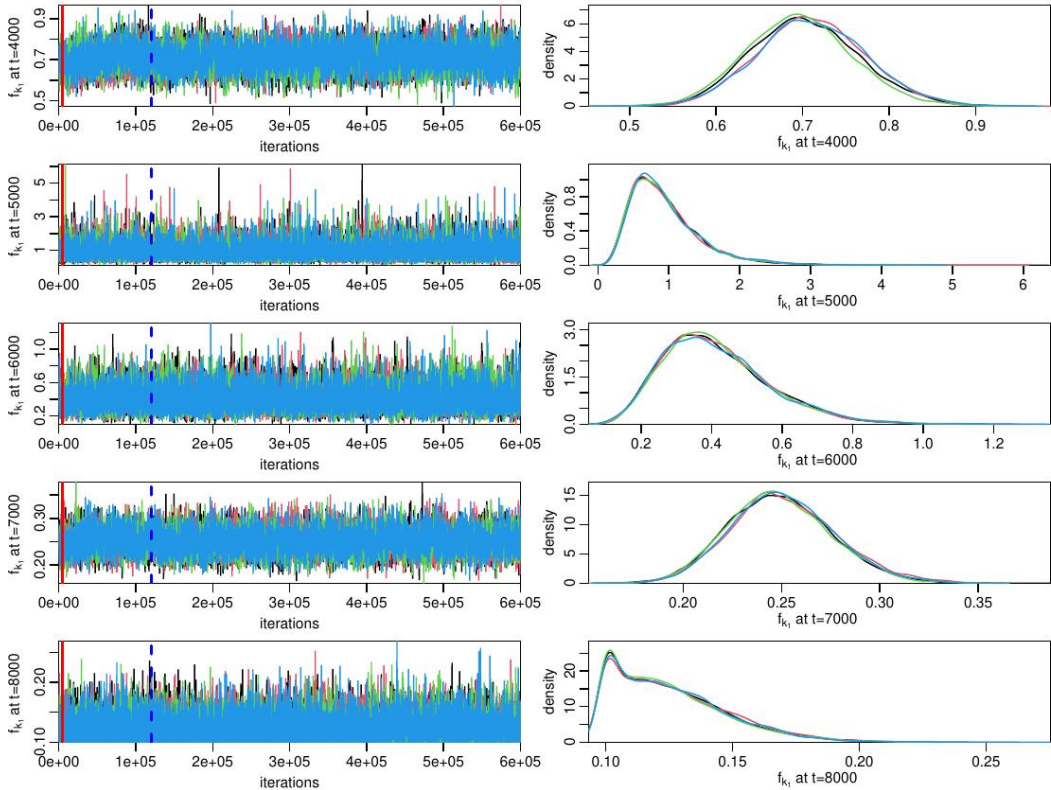


Figure S38. Markov chains and one-dimensional posterior marginals of the time-dependent parameter f_{k_1} at selected points in time for model M2a.

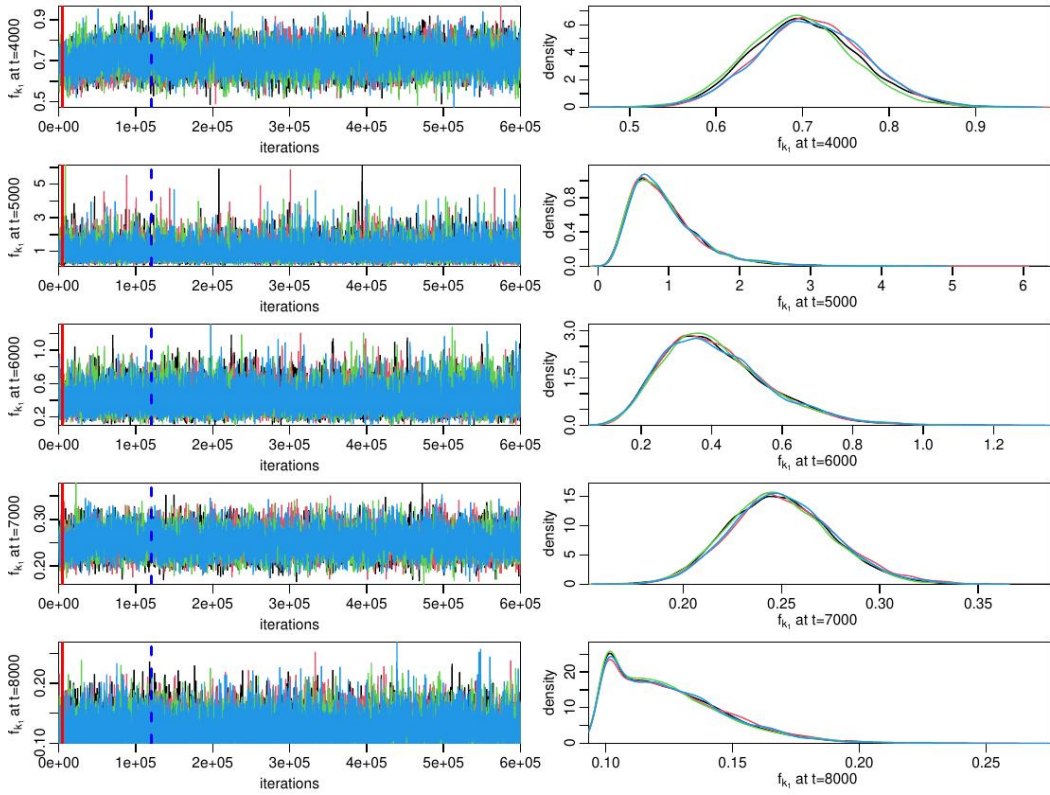


Figure S39. Markov chain and one-dimensional posterior marginals of the time-dependent parameter f_{k_2} at selected points in time for model M2a.

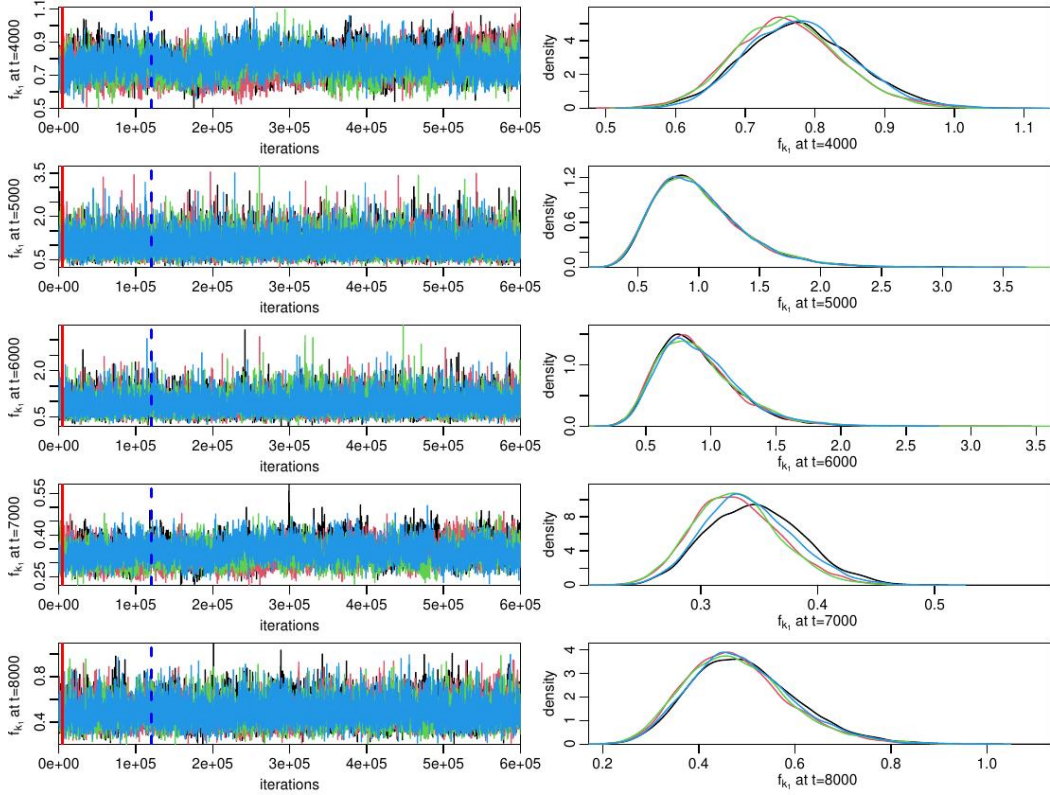


Figure S40. Markov chains and one-dimensional posterior marginals of the time-dependent parameter f_{k_1} at selected points in time for model M2b.

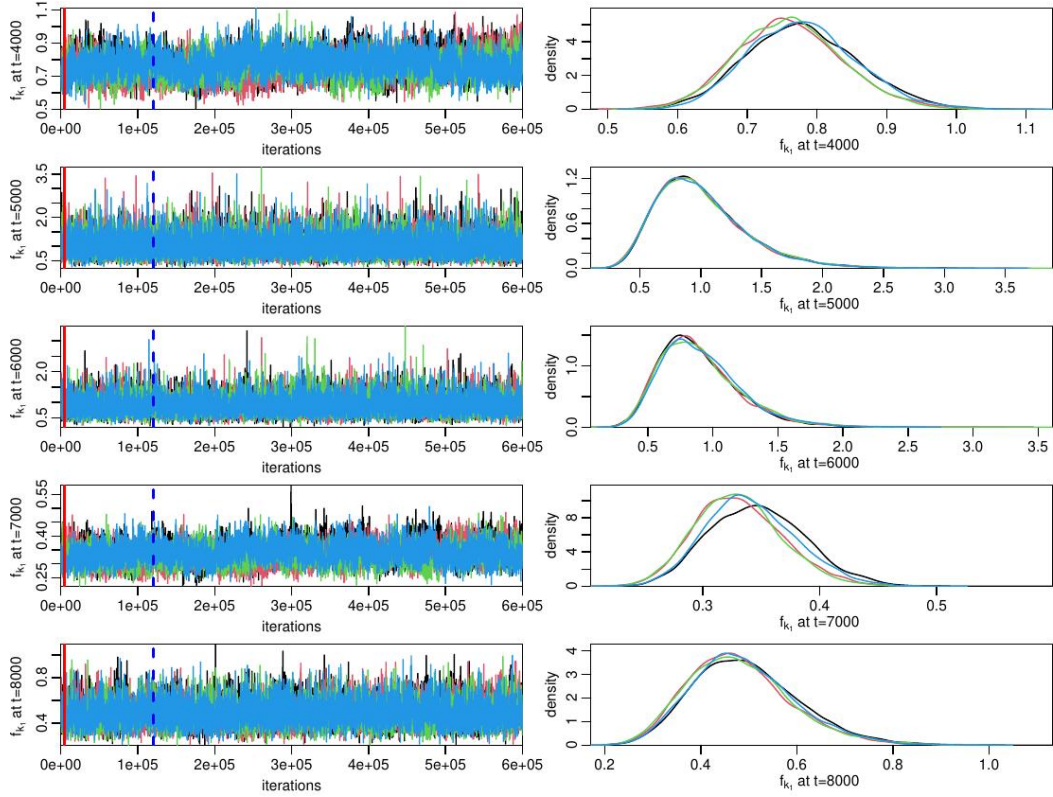


Figure S41. Markov chains and one-dimensional posterior marginals of the time-dependent parameter f_{k_2} at selected points in time for model M2b.

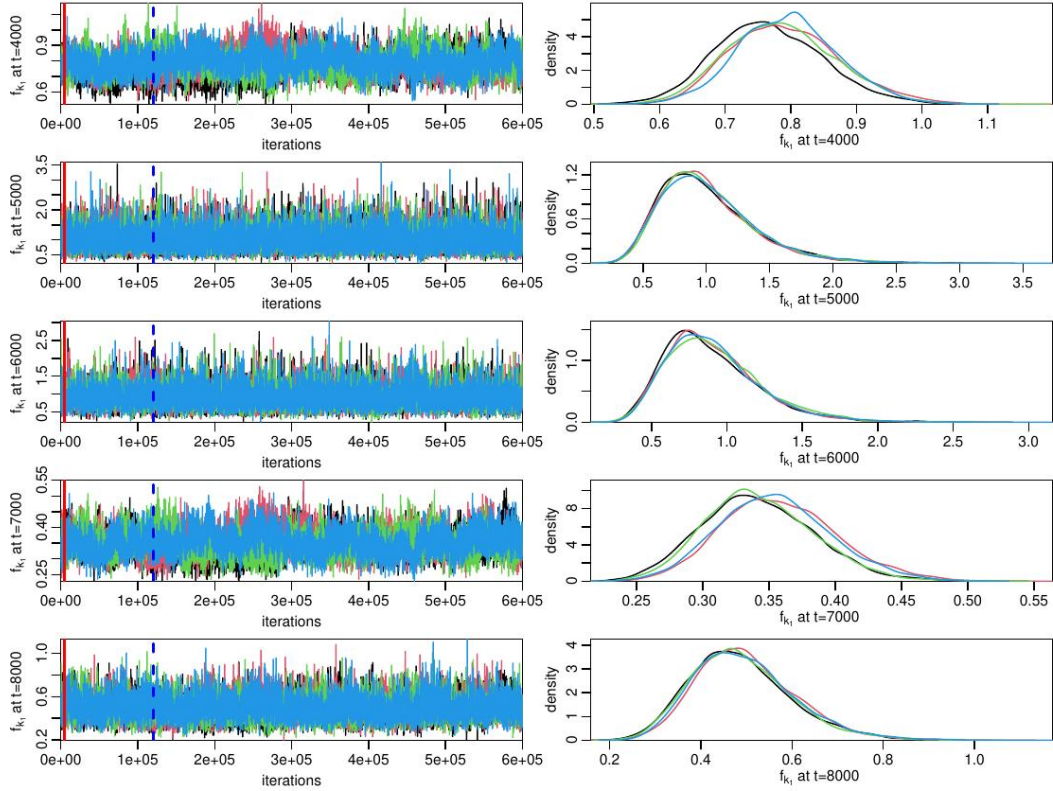


Figure S42. Markov chains and one-dimensional posterior marginals of the time-dependent parameter f_{k_1} at selected points in time for model M2c.

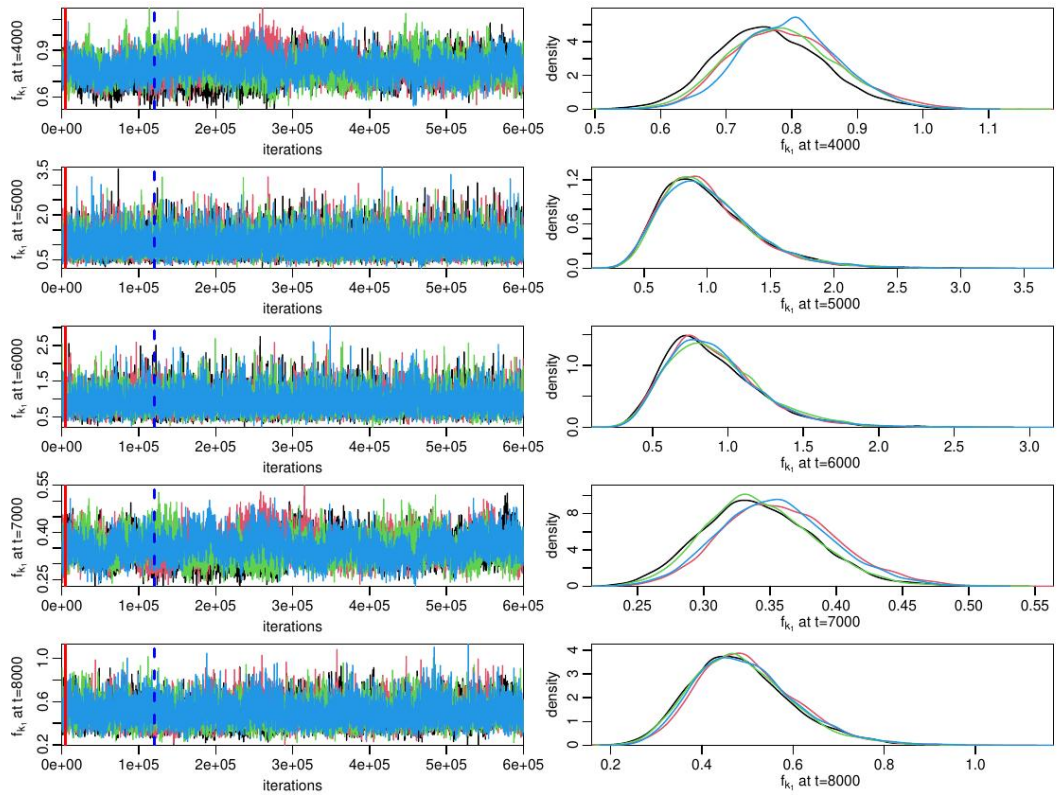


Figure S43. Markov chains and one-dimensional posterior marginals of the time-dependent parameter f_{k_2} at selected points in time for model M2c.

Text S7. Time series of parameters, discharge and water level

The Figures S44 to S48 show the posterior distributions of the time-dependent parameters, discharge and water level for each of the models M1a, M1b, M2a, M2b and M2c with time-dependent parameters over the full calibration and validation time ranges.

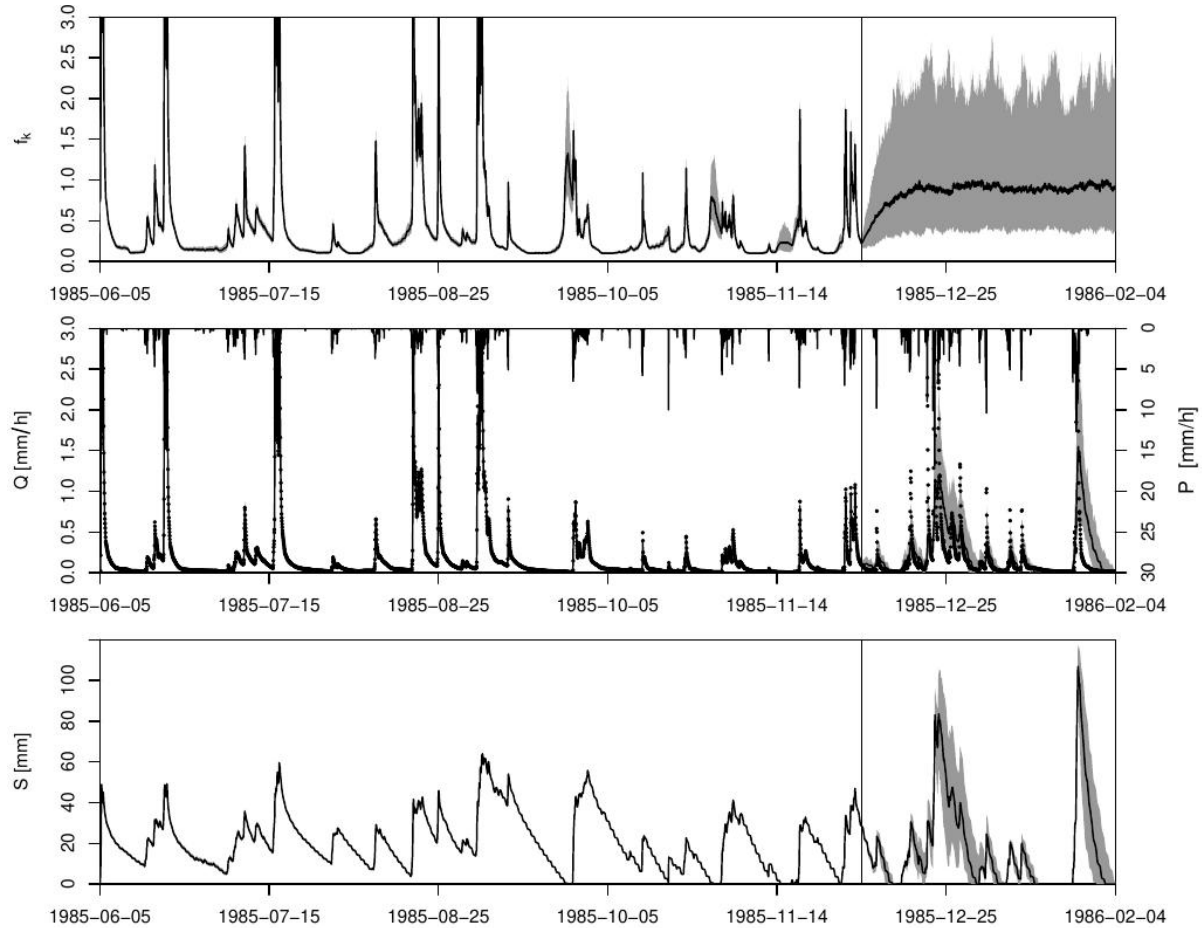


Figure S44. Posterior distribution of the time-dependent parameter, discharge, and reservoir water level for model M1a over the full calibration and validation time ranges.

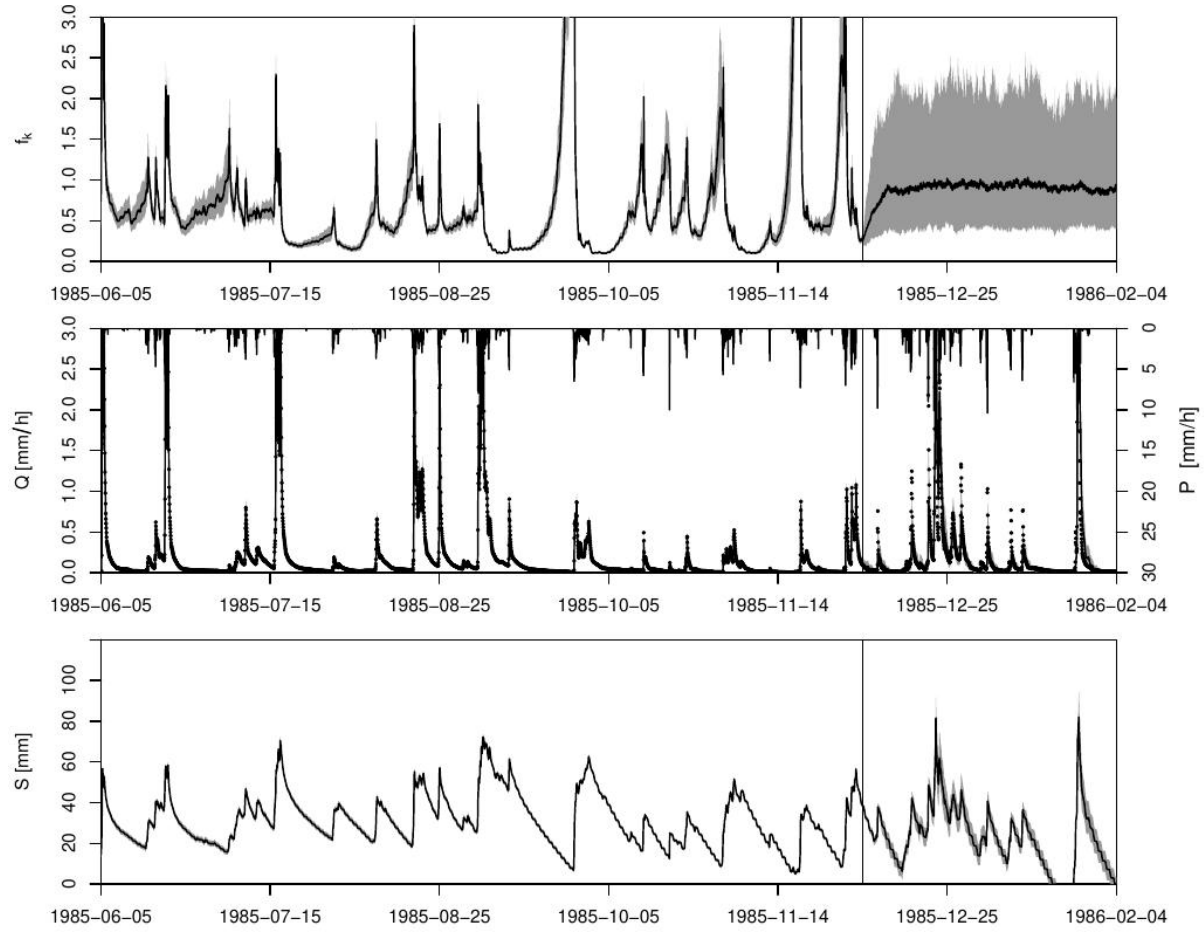


Figure S45. Posterior distribution of the time-dependent parameter, discharge, and reservoir water level for model M1b over the full calibration and validation time ranges.

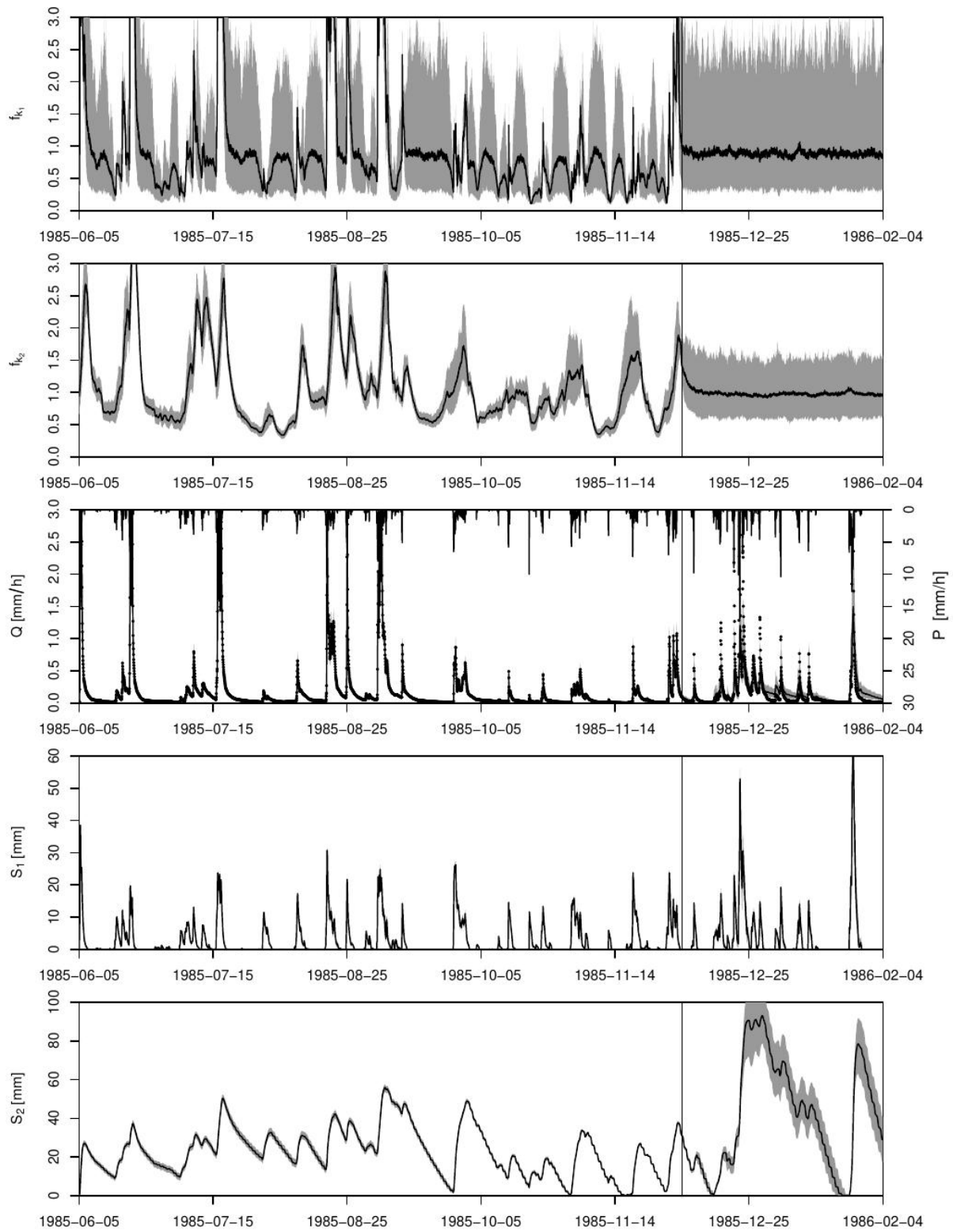


Figure S46. Posterior distribution of the time-dependent parameters, discharge, and reservoir water levels for model M2a over the full calibration and validation time ranges.

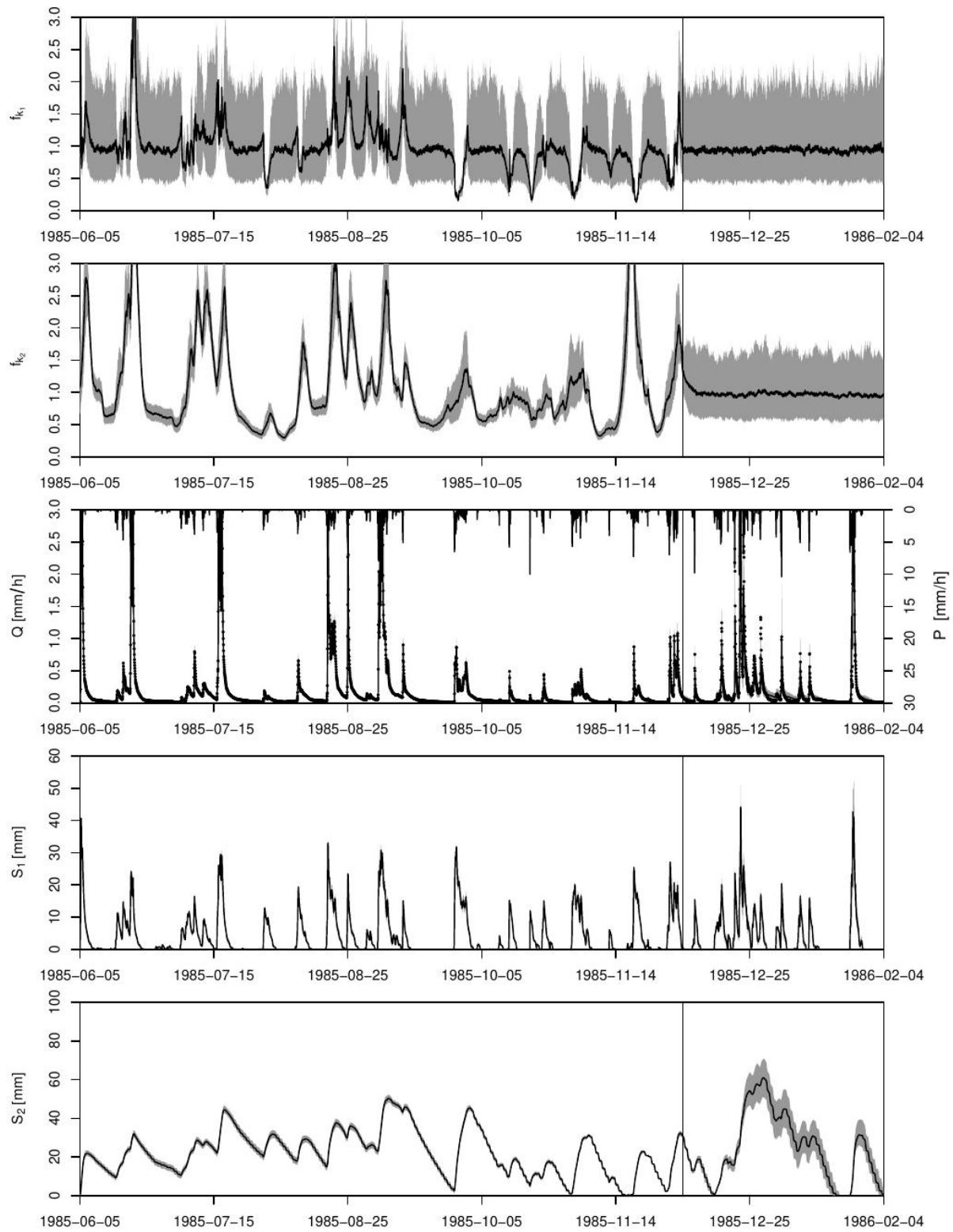


Figure S47. Posterior distribution of the time-dependent parameters, discharge, and reservoir water levels for model M2b over the full calibration and validation time ranges.

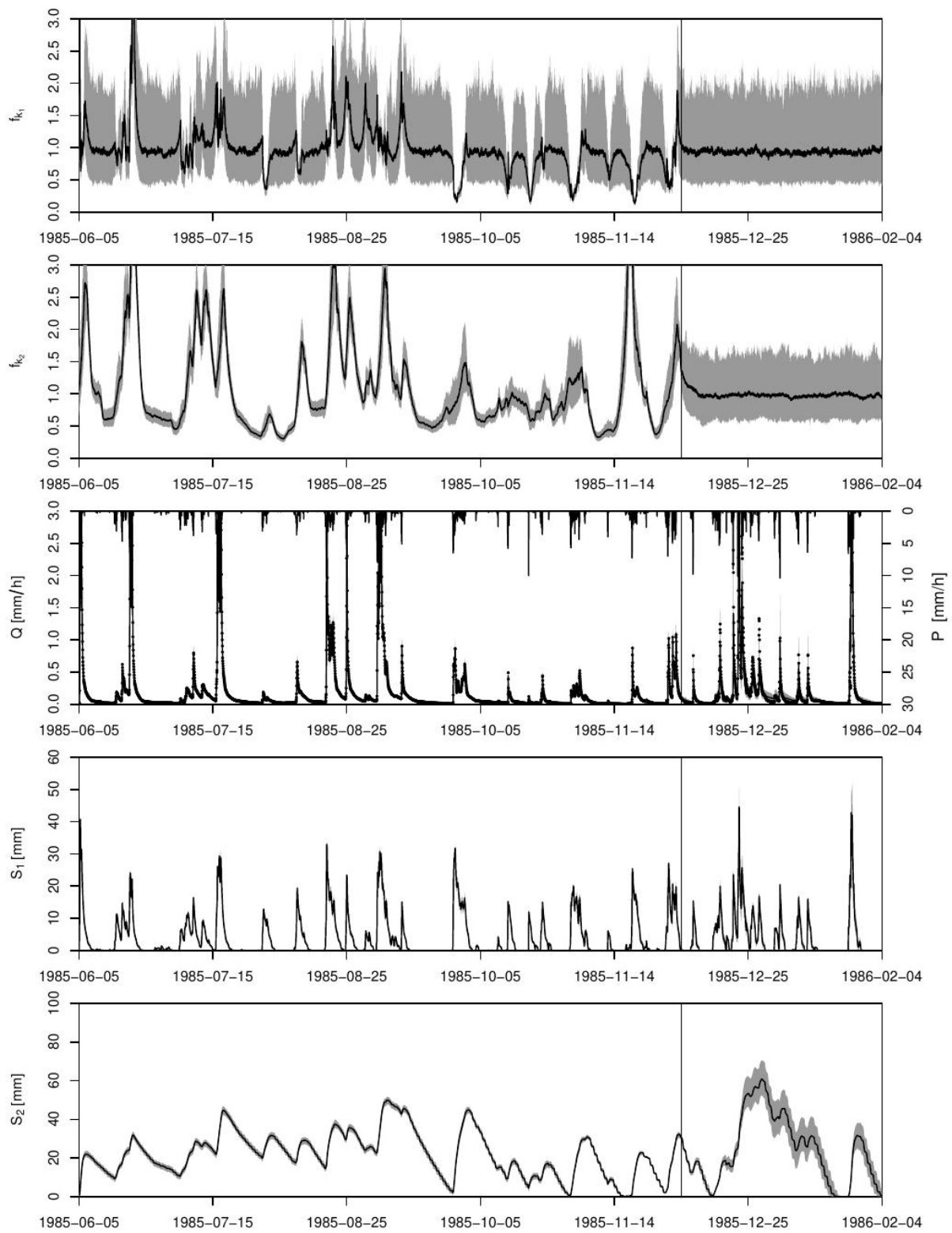


Figure S48. Posterior distribution of the time-dependent parameters, discharge, and reservoir water levels for model M2c over the full calibration and validation time ranges.

The Figures S49 to S53 show the posterior distributions of the time-dependent parameters, discharge and water level and three realizations for each of the models M1a, M1b, M2a, M2b and M2c with time-dependent parameters over the final part of the calibration time range and the first part of the validation time range.

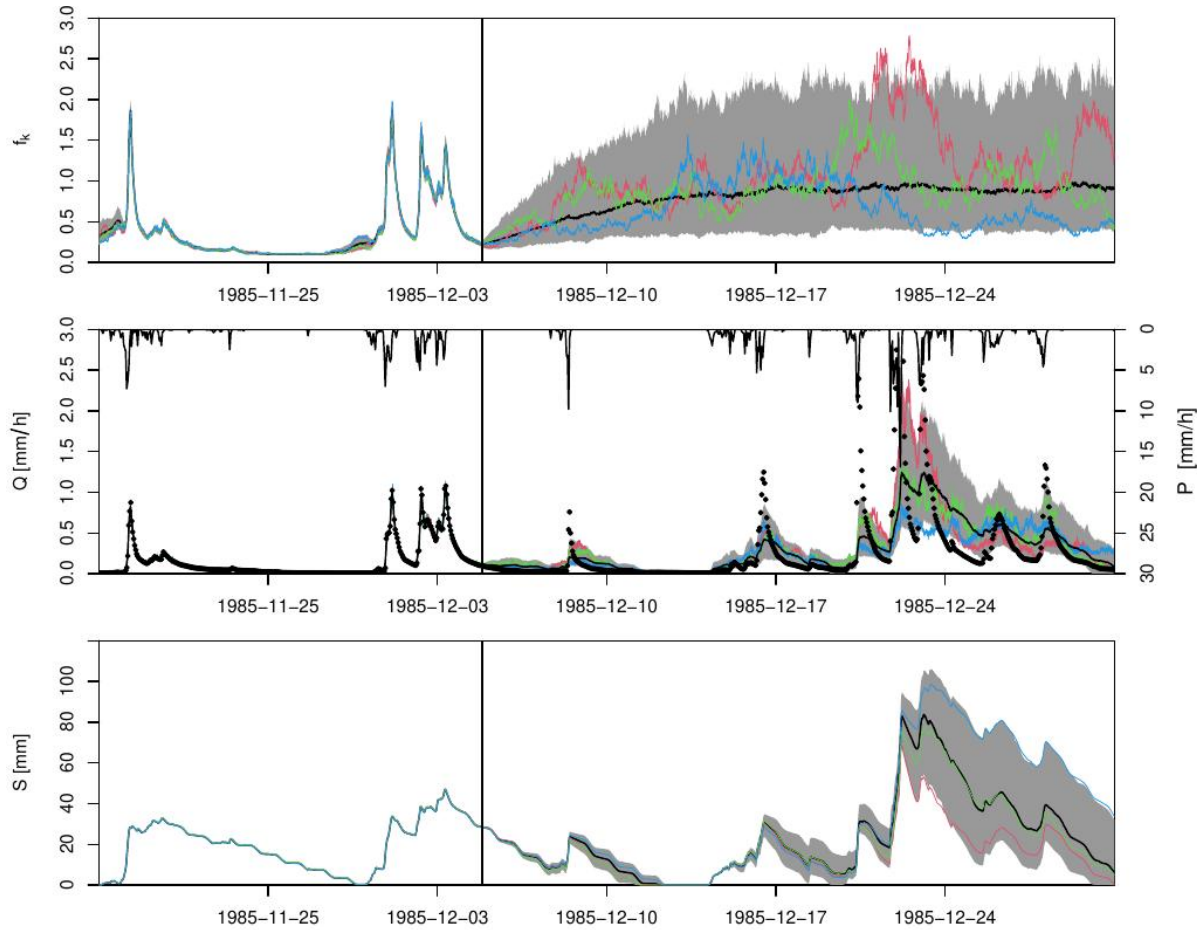


Figure S49. Posterior distribution and three realizations of the time-dependent parameter, discharge, and reservoir water level for model M1a over the final part of the calibration time range and the first part of the validation time range.

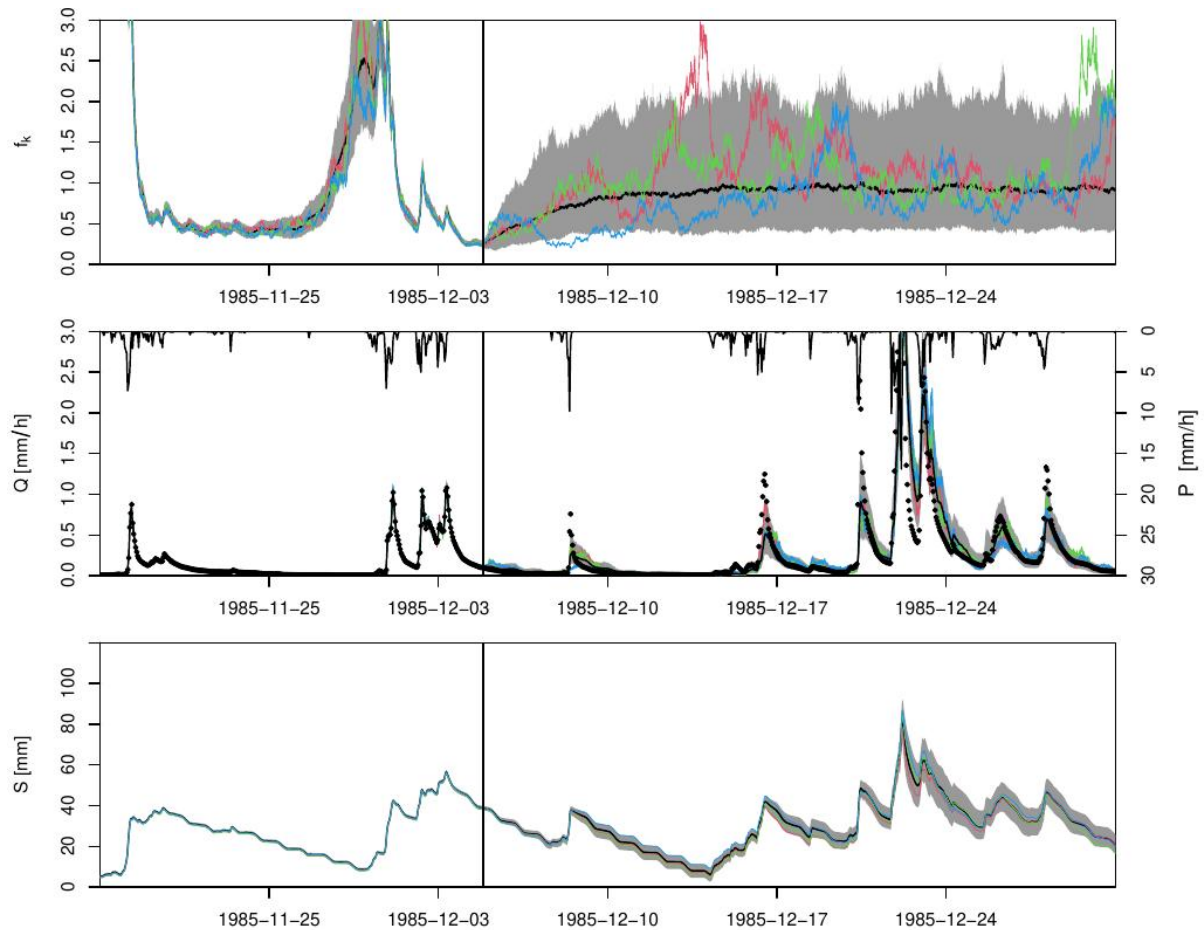


Figure S50. Posterior distribution and three realizations of the time-dependent parameter, discharge, and reservoir water level for model M1b over the final part of the calibration time range and the first part of the validation time range.

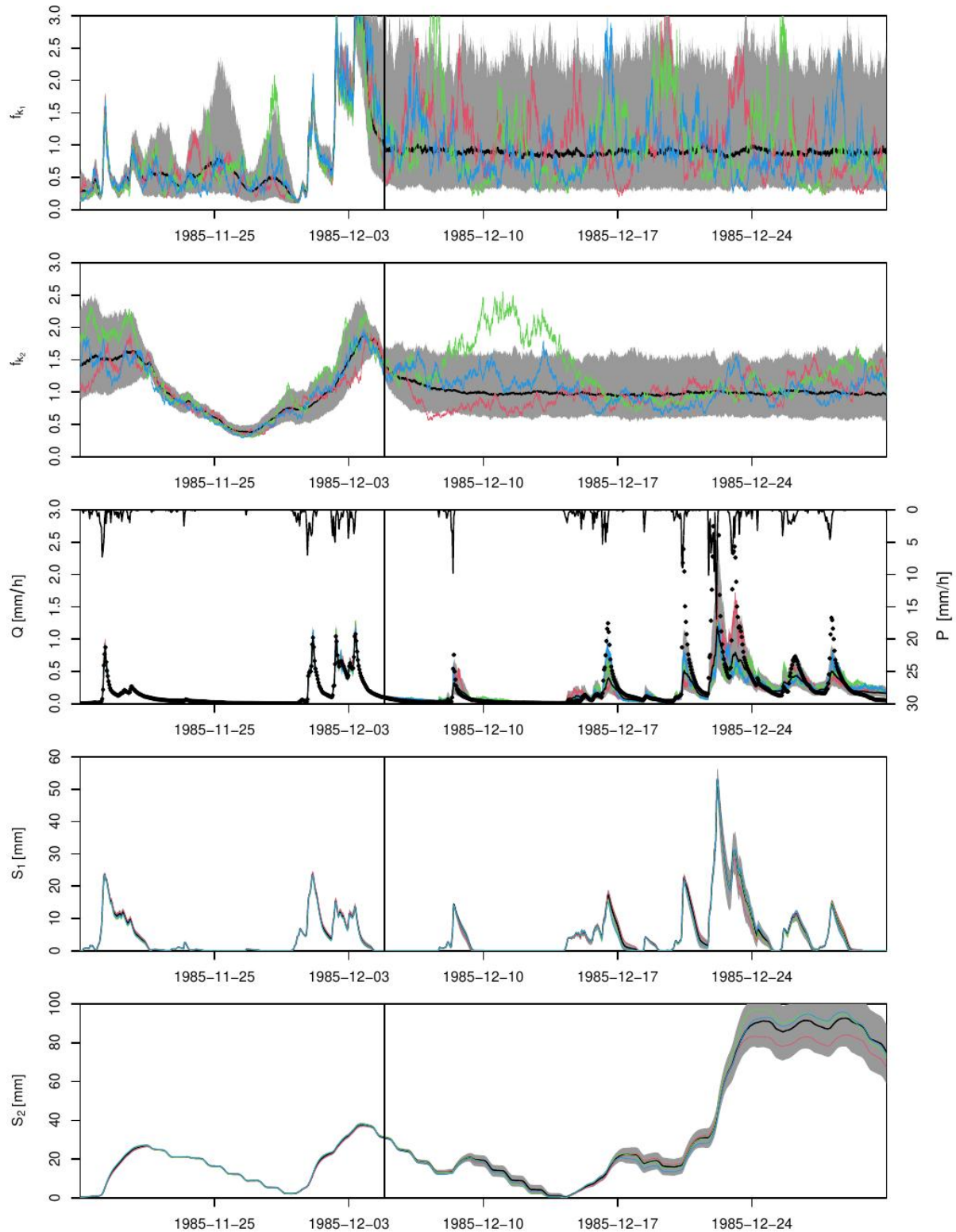


Figure S51. Posterior distribution and three realizations of the time-dependent parameters, discharge, and reservoir water levels for model M2a over the final part of the calibration time range and the first part of the validation time range.

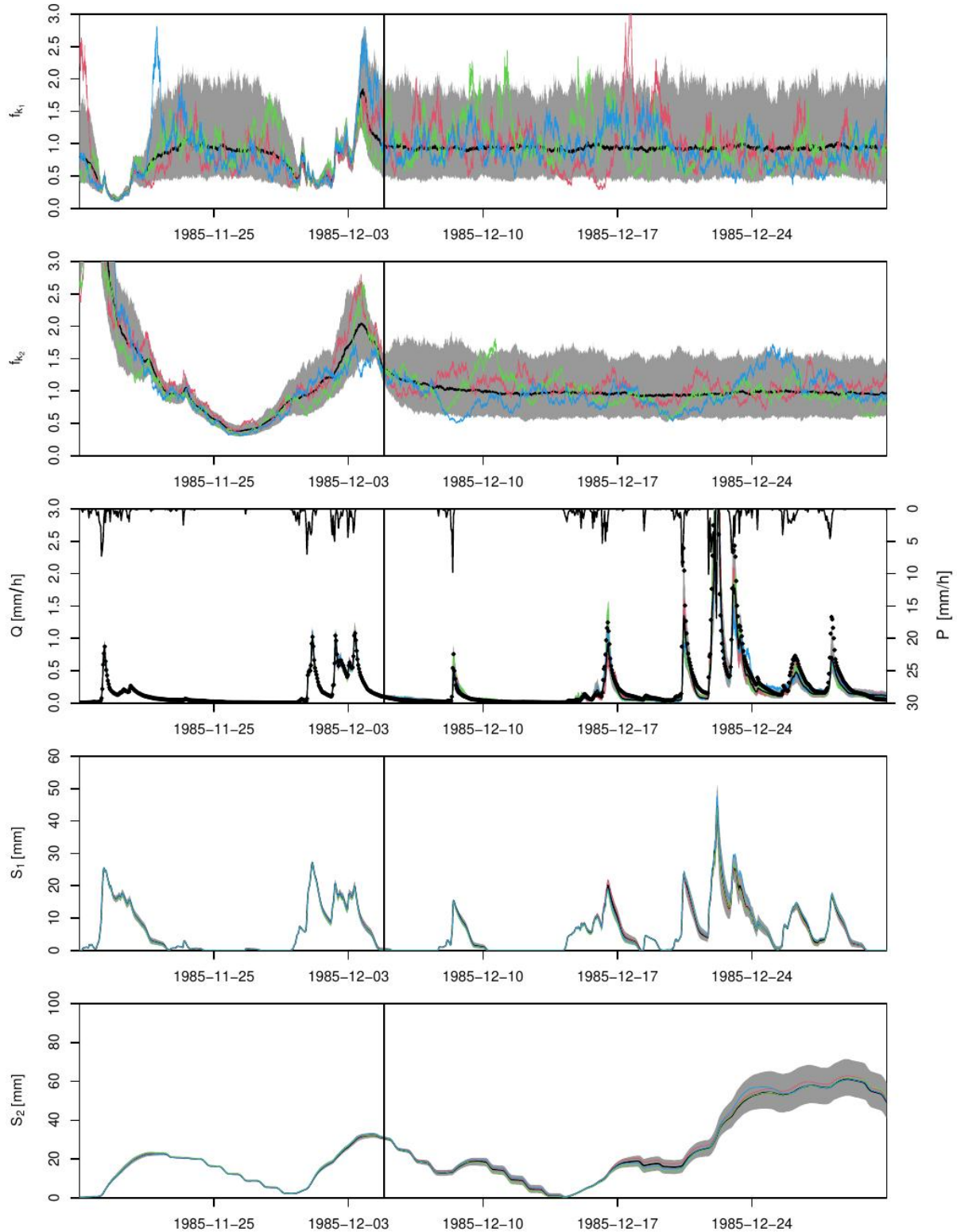


Figure S52. Posterior distribution and three realizations of the time-dependent parameters, discharge, and reservoir water levels for model M2b over the final part of the calibration time range and the first part of the validation time range.

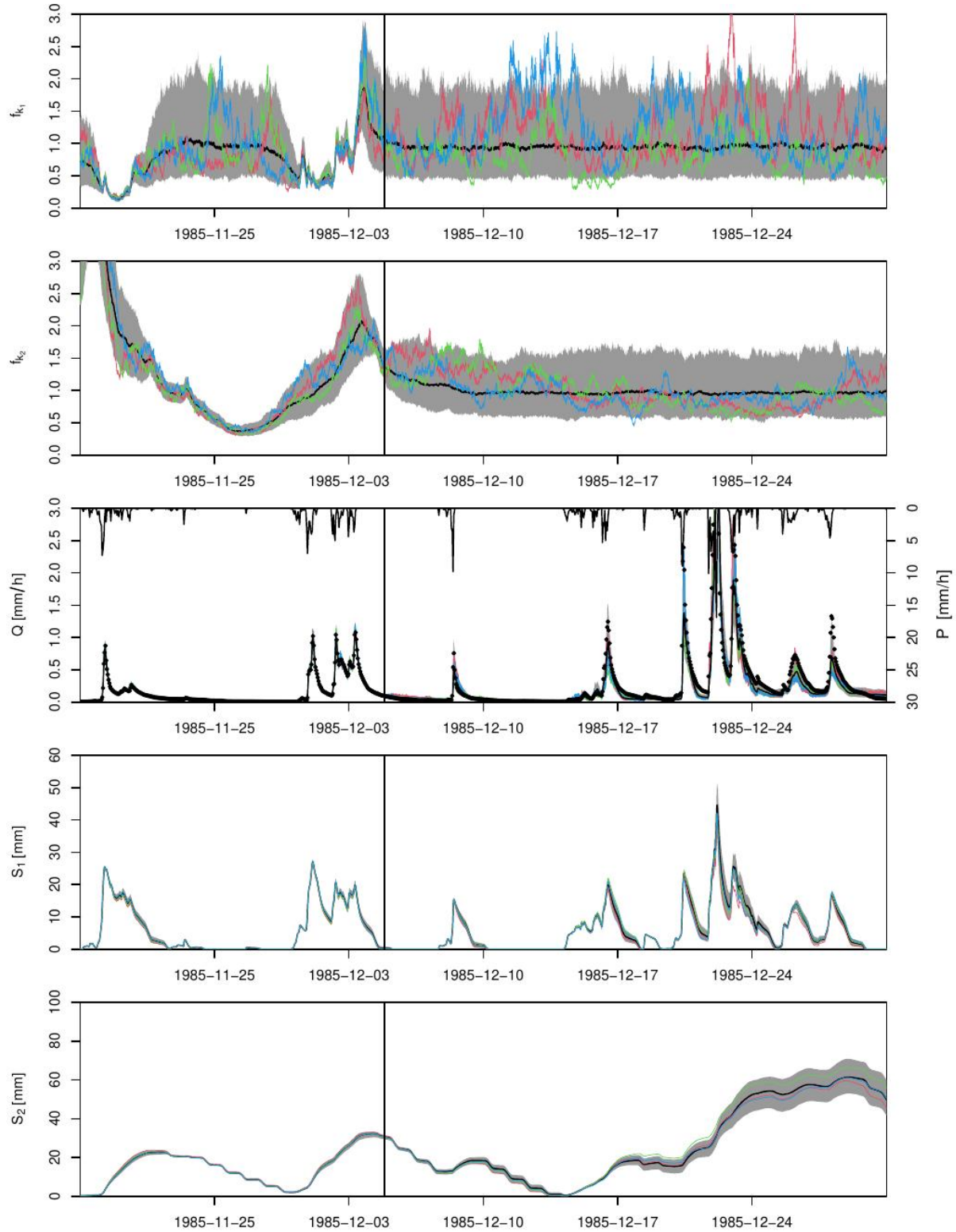


Figure S53. Posterior distribution and three realizations of the time-dependent parameters, discharge, and reservoir water levels for model M2c over the final part of the calibration time range and the first part of the validation time range.

The Figures S54 to S58 show the posterior distributions and three realizations of the time-dependent parameters, discharge and water level for each of the models M1a, M1b, M2a, M2b and M2c with time-dependent parameters over a short part of the validation time range.

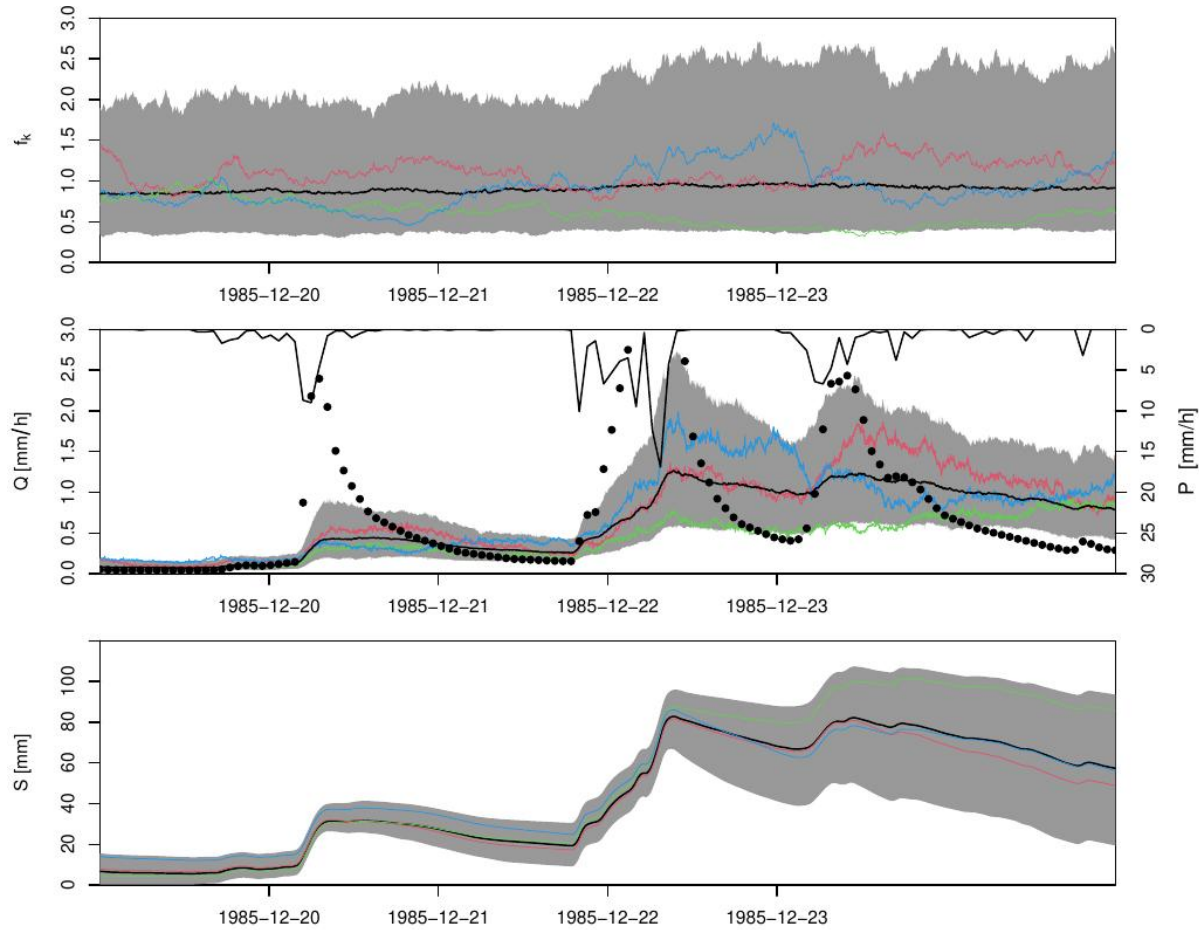


Figure S54. Posterior distribution and three realizations of the time-dependent parameter, discharge, and reservoir water level for model M1a over a short part of the validation time range.

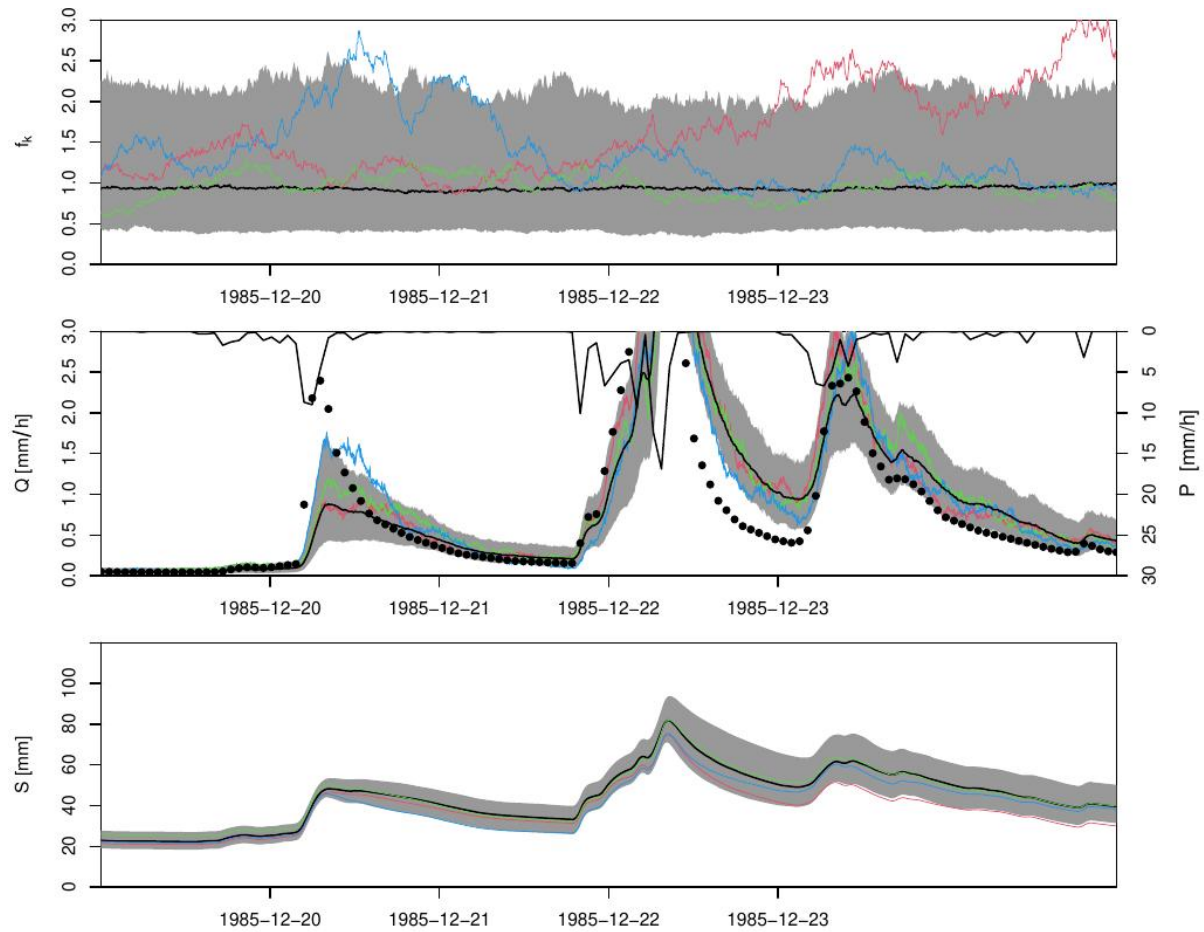


Figure S55. Posterior distribution and three realizations of the time-dependent parameter, discharge, and reservoir water level for model M1b over a short part of the validation time range.

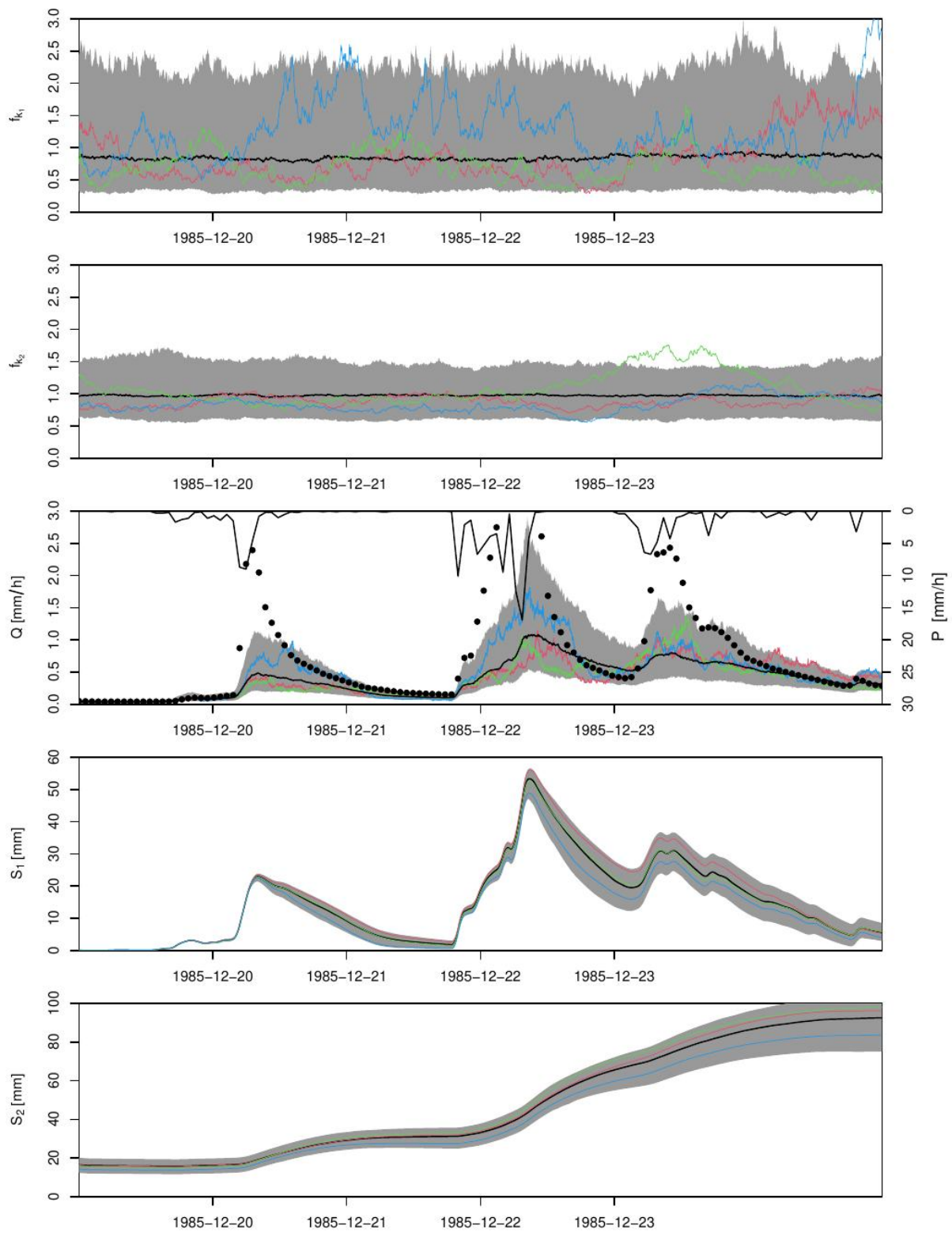


Figure S56. Posterior distribution and three realizations of the time-dependent parameters, discharge, and reservoir water levels for model M2a over a short part of the validation time range.

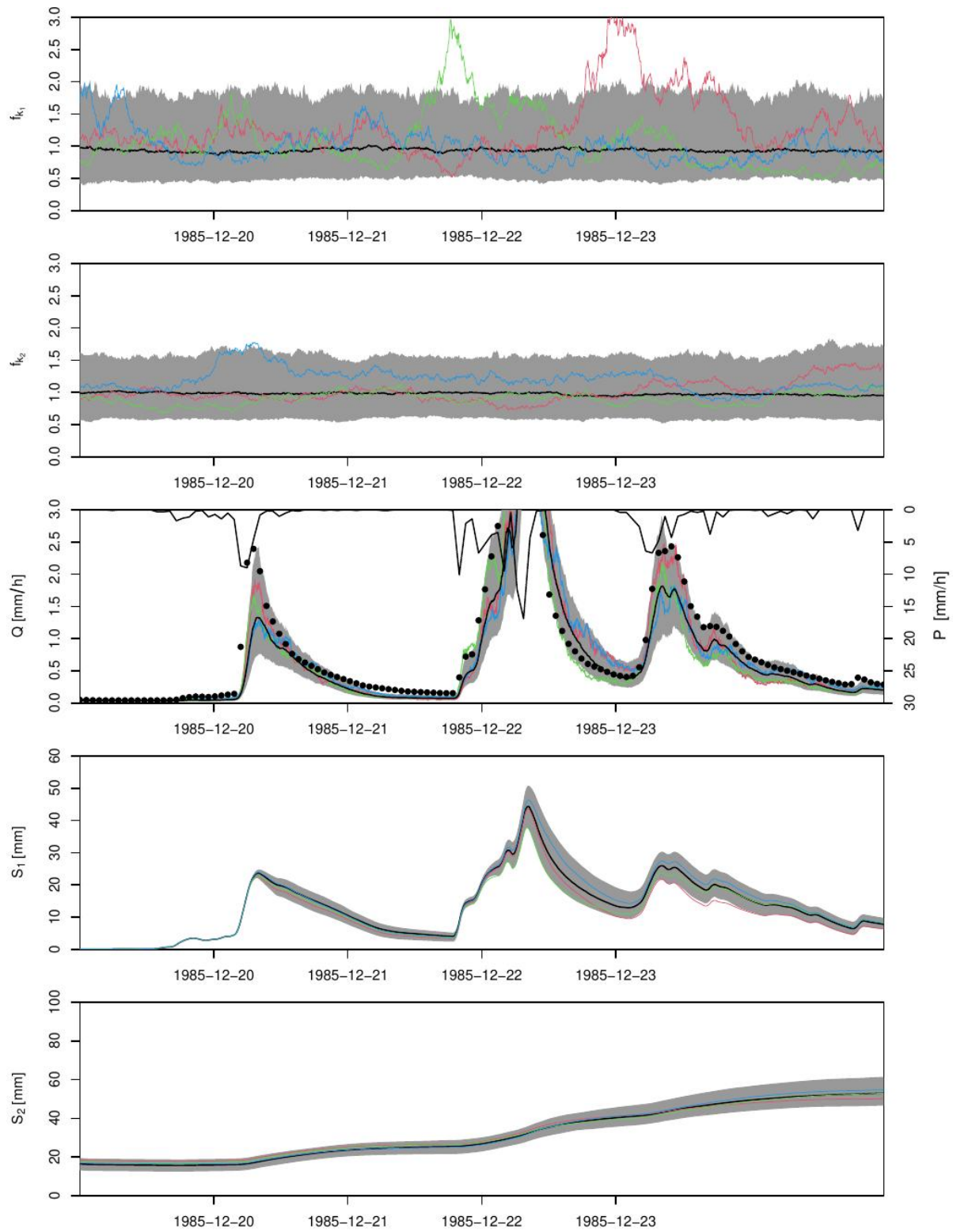


Figure S57. Posterior distribution and three realizations of the time-dependent parameters, discharge, and reservoir water levels for model M2b over a short part of the validation time range.

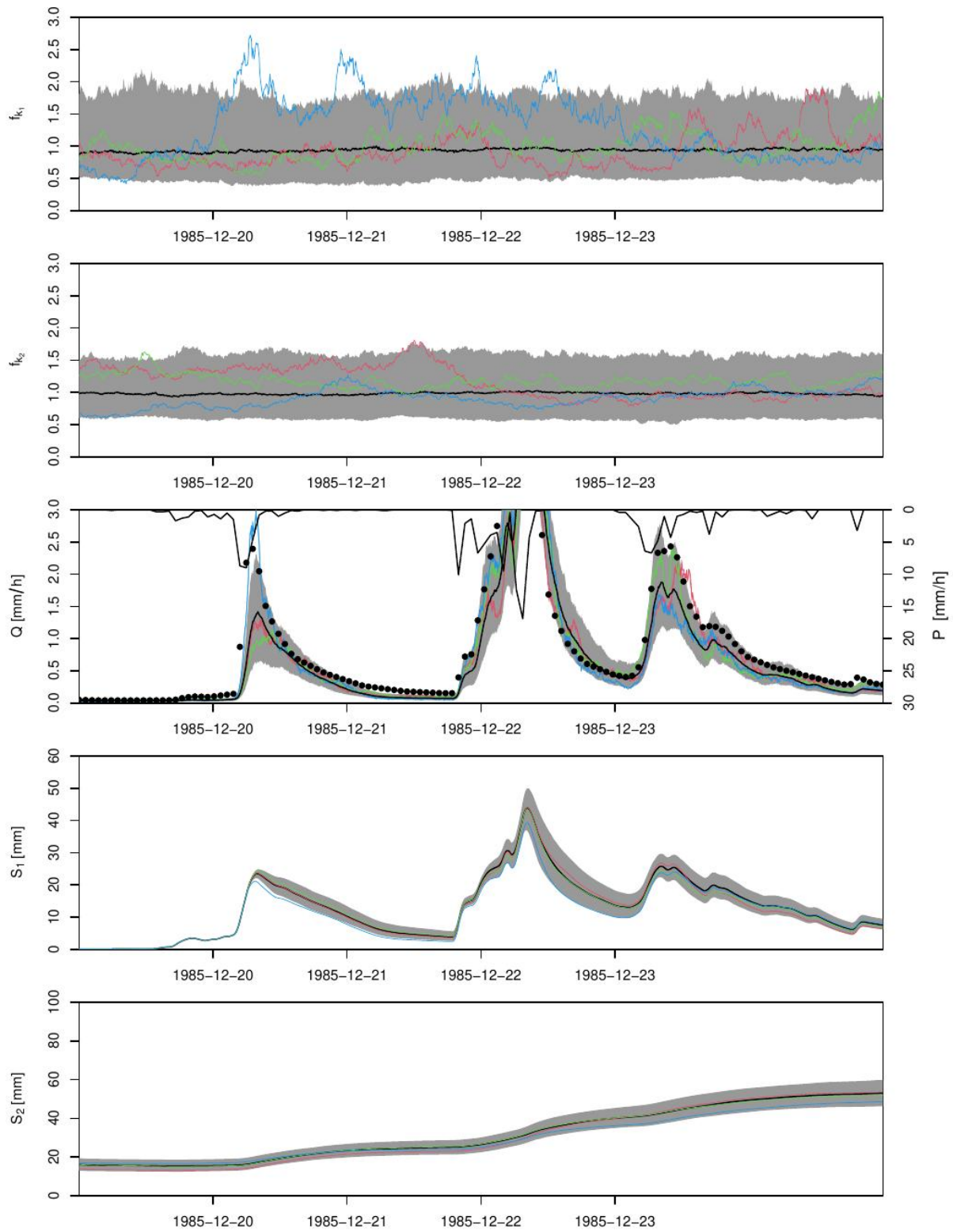


Figure S58. Posterior distribution and three realizations of the time-dependent parameters, discharge, and reservoir water levels for model M2c over a short part of the validation time range.

Text S8. Scatter plots of f_k , f_{k_1} and f_{k_2} versus S , S_1 and S_2

Figure S59 shows the complete set of scatter plots of f_k , f_{k_1} and f_{k_2} versus S , S_1 and S_2 .

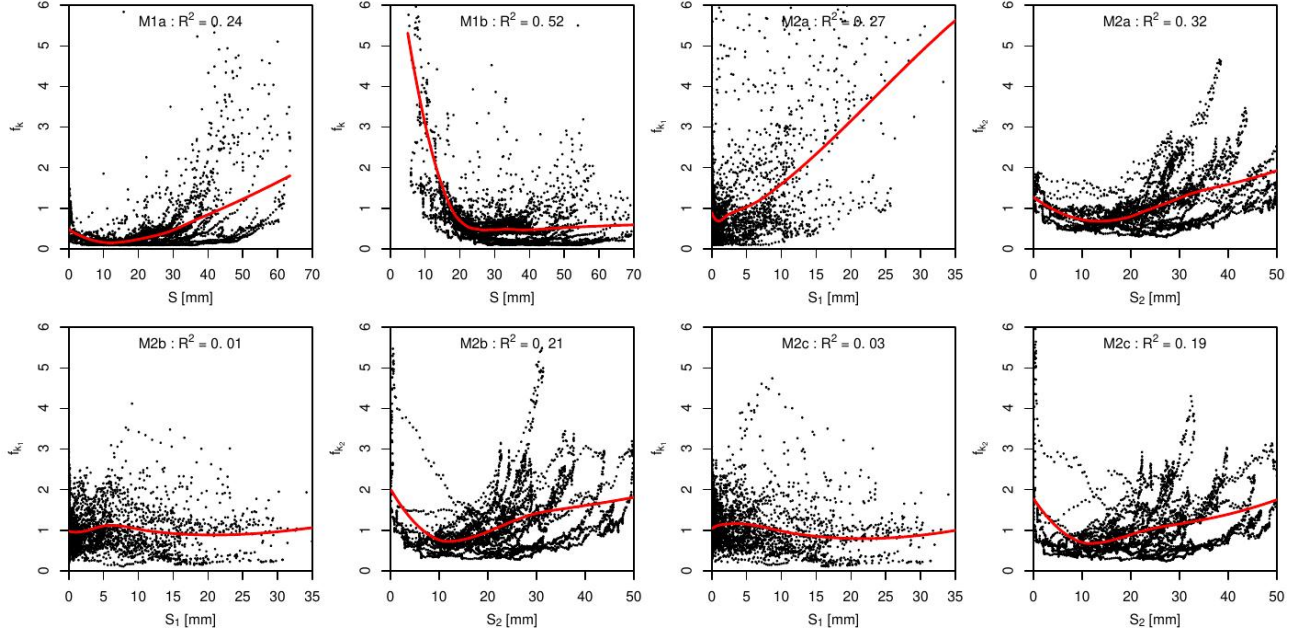


Figure S59. Scatter plot of the time-dependent parameters (multipliers), f_k versus the reservoir level S for the models M1a and M1b, and f_{k_1} and f_{k_2} versus the reservoir levels S_1 and S_2 , respectively, for the models M2a, M2b and M2c. The red line indicates a potential relationship between the variables produced with a smoothing algorithm implemented in the R function `loess`. The value of R^2 at the top of the plots shows the degree of variance reduction achieved by the smoothing model.